

PAPER • OPEN ACCESS

A novel understanding of the role of plasma-molecular kinetics on divertor power exhaust

To cite this article: N. Osborne *et al* 2025 *Nucl. Fusion* **65** 116010

View the [article online](#) for updates and enhancements.

You may also like

- [Triangularity dependence of the divertor heat flux profile and SOL filamentary turbulence on TCV](#)
R.I. Morgan, G. Durr-Legoupil-Nicoud, O. Février *et al.*
- [Orbit-space sensitivity of two-step reaction gamma-ray spectroscopy](#)
A. Valentini, H. Järleblad, M. Nocente *et al.*
- [A compact fusion reactor based on the staged compression of a field reversed configuration](#)
John Slough



Speed Up the Development of Fusion Technology with Multiphysics Simulation

Generate clean energy more efficiently.

To improve the production of fusion energy and help pave the way to using it as a commercial power source, engineers are using multiphysics simulation for the development of fusion systems.

Simulation enables engineers to observe the complex phenomena in their systems, predict performance and reduce testing and production times.

» comsol.com/industry/energy/nuclear

COMSOL

A novel understanding of the role of plasma-molecular kinetics on divertor power exhaust

N. Osborne^{1,3,*} , K. Verhaegh² , D. Moulton¹ , S. Mijin¹ , H. Reimerdes⁴ , P. Ryan¹ , N. Lonigro^{1,5} , R. Osawa¹ , K. Murray^{1,3} , S. Kobussen² , Y. Damizia⁶ , A. Perek⁴ , C. Theiler⁴ , R. Ducker⁴ , D. Mykytchuk⁴ , the Eurofusion Tokamak Exploitation Team^a, the MAST-U Team^b and the TCV Team^c

¹ UKAEA, Culham Campus, Abingdon OX14 3DB, United Kingdom of Great Britain and Northern Ireland

² Eindhoven University of Technology, Eindhoven, Netherlands

³ University of Liverpool, Liverpool, United Kingdom of Great Britain and Northern Ireland

⁴ Swiss Plasma Centre, École Polytechnique Fédérale de Lausanne, Lausanne, Switzerland

⁵ York Plasma Institute, University of York, York, United Kingdom of Great Britain and Northern Ireland

⁶ The College of William & Mary, Williamsburg, VA, United States of America

E-mail: nick.osborne@ukaea.uk

Received 12 May 2025, revised 20 August 2025

Accepted for publication 22 September 2025

Published 6 October 2025



CrossMark

Abstract

During detachment, a buffer of neutral atoms and molecules builds up between the target and the ionising plasma. Collisions between the plasma and the molecules play an important role in the detachment process. Studies of plasma-molecular kinetics indicate that the gas temperature increases during deepening detachment for a wide range of conditions on the MAST-U and TCV tokamaks. This is related to an increased D₂ lifetime during detachment, leading to more plasma-molecule collisions that raise the molecular temperature. Such collisions subsequently result in power and momentum losses from the divertor plasma during detachment. Using a simplified inference, these losses are estimated using the rotational temperature, neutral pressure and ionisation front position. Significant power losses (about 10% of P_{SOL}) and dominant momentum losses (majority of the upstream pressure) from plasma-molecule collisions are inferred experimentally in long-legged, strongly baffled, detached divertors (MAST-U Super-X divertor). These findings are consistent with SOLPS-ITER simulations (about 15% of P_{SOL} , and 65% of upstream pressure). Simulations also suggest that 40%–50% of the power crossing the ionisation front is lost downstream. The vibrational distribution obtained is compared with a collisional-radiative model setup using the same rate data as SOLPS-ITER,

^a See Joffrin *et al* 2024 (<https://doi.org/10.1088/1741-4326/ad2be4>) for the EUROfusion Tokamak Exploitation Team.

^b See Harrison *et al* 2019 (<https://doi.org/10.1088/1741-4326/ab121c>) for the MAST-U Team.

^c See Duval *et al* 2024 (<https://doi.org/10.1088/1741-4326/ad8361>) for the TCV Team.

* Author to whom any correspondence should be addressed.



Original Content from this work may be used under the terms of the [Creative Commons Attribution 4.0 licence](https://creativecommons.org/licenses/by/4.0/). Any further distribution of this work must maintain attribution to the author(s) and the title of the work, journal citation and DOI.

indicating some qualitative agreements and disagreements, potentially highlighting model gaps with regard to the default rates used. These interpretations highlight the importance of plasma-molecular collisions, leading to power and momentum losses during detachment.

Keywords: MAST-U, TCV, D2, plasma-molecule, fulcher emission, detachment, divertor

(Some figures may appear in colour only in the online journal)

1. Introduction

Plasma detachment will be a feature of future reactors to ensure that both divertor target electron temperature and heat flux are reduced by the orders of magnitude necessary [1, 2]. During detachment, plasma-neutral interactions (collisions and reactions) are key in the required removal of power, momentum and ions from the plasma [3–7]. Plasma-molecule interactions, specifically, have now been shown to play a crucial role in detachment in several experimental devices [4, 8–10].

Figure 1, which shows an unfurled scrape-off-layer from mid-plane to divertor target, indicates the different processes present during detachment. From upstream to downstream along the divertor leg, we pass from the ionisation region, through the neutral cloud where plasma-atom and plasma-molecule interactions occur, to the electron-ion recombination region closest to the target [11].

The upstream edge of the neutral cloud, just below (downstream of) the ionisation region, corresponds with a peak in Fulcher emission from the molecules, as is well established by measurements and emission modelling in both MAST-U and TCV [8, 11]. Fulcher emission is a visible band of spectral lines between ~ 600 nm and ~ 640 nm emitted by electronically excited hydrogen molecules transitioning from the upper Fulcher state ($d^3\Pi_u^-$) to the lower Fulcher state ($a^3\Sigma_g^+$) and is very useful as a diagnostic tool. It is at this edge where there starts to be a significant number of molecules but still enough hot electrons to electronically excite the molecules. In this paper, we refer to this region of peak Fulcher emission as the ‘detachment front’ in keeping with other works where the same region is used to diagnose [10, 12, 13] and even control [14] detachment on MAST-U.

In detached conditions ($T_e < 3 - 5$ eV), ion-molecule collisions have been found to be a dominant mechanism for power and momentum losses in MAST-U SOLPS-ITER simulations [15]. Meanwhile, in the same detached conditions, reactions in the form of molecular chain chemistry processes are dominated by ion sinks (Molecular Activated Recombination or MAR) and neutral sources (Molecular Activated Dissociation or MAD) [8, 16]. This highlights the importance of plasma-molecule interactions in the detachment process.

The same D₂ Fulcher emission which indicates the detachment front, can be monitored *in high spectral resolution*, allowing for careful study of the molecules’ rotational and vibrational, or ‘rovibrational’, distribution. This measurement provides information on both collisions between the plasma

and the molecules via the rotational distribution (rotational temperature); and information on the likelihood of the plasma to undergo molecular chain chemistry processes, which favour highly vibrationally excited molecules, via the vibrational distribution.

Diagnosing the rovibrational distribution of D₂ molecules is, therefore, potentially very useful in providing insight into the plasma-molecule interactions which are so fundamental in detachment.

Specifically, we have found that increasing rotational, or gas, temperature is a signature of energy transfer from the plasma to the molecules through collisions, the same process that drives momentum losses during detachment. Meanwhile, the vibrational distribution directly drives effective molecular charge exchange rates and affects molecular ionisation rates [17–19]. These are the first stages in the MAR and MAD processes described above and, hence, the vibrational distribution plays a role in these processes.

1.1. Historical work

Investigations on tokamaks (JET [20], DIII-D [21], ASDEX-Upgrade [22] and JT60-U [23]), and other devices such as LHD [24] and Magnum-PSI [25], have inferred rotational temperatures for the ground-state of D₂ between approximately 1000 K and 10 000 K. Measurements on JET [20], DIII-D [21] and LHD [24], suggest a correlation of rotational temperature with electron density, and Hollmann *et al* [21] shows that, at the same electron density on DIII-D, TEXTOR, and PISCES (linear device), similar rotational temperatures are measured. Recent work on two metal-walled devices (QUEST and LTX- β) and carbon-walled DIII-D by Yoneda *et al* [26] suggests a high sensitivity of rotational temperature to electron density and attempts to predict the rotational temperature increases by use of a collisional-radiative model with 858 differential equations. The same study indicated a low sensitivity to electron temperature, at least in plasma regimes above 10 eV.

Previous experiments [21, 27–30] inferred a vibrational temperature of the molecular ground-state by using Franck-Condon coefficients to map an assumed vibrational temperature in the ground state to the electronically-excited Fulcher level. Results on JET-ILW [20], however, feature an overpopulated $\nu = 0$ band in the excited Fulcher level, suggesting a strongly non-Boltzmann ground state with highly overpopulated $\nu = 1, 2, 3$. TEXTOR results (carbon surface) [30] found an overpopulation of the $\nu = 3$ band and thus an imperfect fit with a ground state Boltzmann distribution.

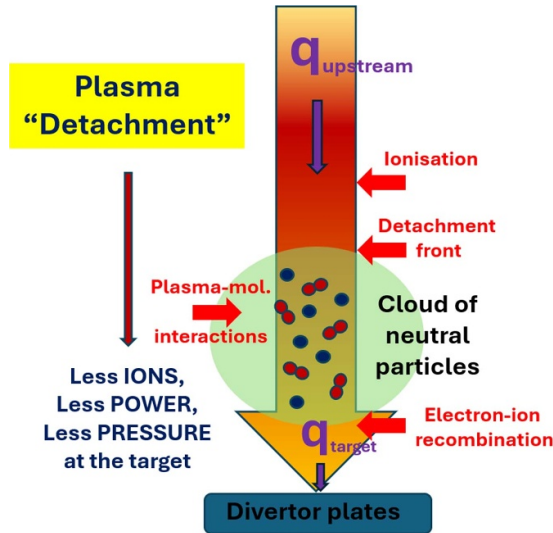


Figure 1. Simplified representation of the scrape-off-layer from mid-plane to divertor target in a deeply detached plasma.

Our previous work [13], studied the MAST-U [31] divertor in Ohmic density ramp discharges and found rotational temperatures consistent with these previous findings. The rotational temperature was found to increase in deep detachment in the strongly baffled MAST-U divertor, hinting at a connection to longer lifetimes of the molecules before dissociation or ionisation. Our MAST-U results also demonstrated a non-Boltzmann distribution for the ground-state vibrational distribution of the molecules, and revealed a curious boost to the $\nu = 2, 3$ populations during detachment [13].

1.2. This paper

In this work high spectral resolution D_2 & H_2 Fulcher band emission is obtained in long-legged divertors of both MAST-U and TCV [32] to extract the rotational and vibrational (rovibrational) distribution of the molecules.

We investigate how information from the **rovibrational distribution** of D_2 & H_2 can provide more insight into plasma-molecule interaction in a long-legged divertor. Specifically we note the following outcomes:

1. A better understanding of the mechanism behind the increase in rotational temperature as detachment progresses;
2. Quantification of power and momentum losses due to plasma–molecule collisions;
3. Comparison of the vibrational distribution with collisional–radiative models, noting its bearing on plasma chemistry.

Going beyond our previous ohmic MAST-U work [13], this study uses the unique features of both the MAST-U and TCV tokamaks to obtain improved insights into what impacts plasma-molecular kinetics. The following features are varied:

- Divertor configuration, e.g. variations in poloidal leg length and total flux expansion (MAST-U), to investigate the impact of divertor leg length on plasma-molecular kinetics.
- Baffled and unbaffled conditions (TCV), to investigate the impact of neutral closure and trapping in the divertor on plasma-molecular kinetics.
- Fuelling location and fuelling strength (TCV and MAST-U), to investigate their impact on plasma-molecular kinetics.
- Fuelling species (isotopic variation) (H_2 in TCV), to investigate the impact of different isotopes on plasma-molecular kinetics.
- External heating levels (MAST-U with/without NBI heating) to investigate the impact of external heating on plasma-molecular kinetics in the divertor.
- L- and H-mode (MAST-U), to investigate whether regular transients (ELMs in H-mode) have an impact on plasma-molecular kinetics in the inter-ELM/‘baseline’ state.

We find that the observed behaviour of the rotational and vibrational distribution of hydrogenic molecules, in response to the above variations, is similar on MAST-U and TCV. For all conditions, the rotational temperature rises during and near detachment. For both TCV and MAST-U, this increase in rotational temperature is correlated with an enhancement of the $\nu = 2, 3$ population in the upper Fulcher state.

This work provides novel insights into the importance of plasma-molecule collisions on detachment. A reduced model explains the observed rotational temperature increase, consistent with SOLPS-ITER simulations: the energy transfer from the plasma to the molecules is enhanced in detached conditions as the lifetime of the molecules is increased. Collisions between the plasma and the molecules result in significant power loss (up to $>10\%$ of P_{SOL} , the power entering the Scrape-Off-Layer); and losses of up to $>40\%$ downstream of the ionisation front); and very significant momentum sinks.

The measured vibrational distribution is yet to be accurately reproduced by collisional-radiative modelling which employ the same plasma-molecular rates used in exhaust simulations. This mismatch increases uncertainty in the rates used, and motivates more experimental and modelling studies.

2. Experimental setup

Both MAST-U and TCV have clean intersections between the spectroscopic lines-of-sight and the divertor plasma. Furthermore, both devices support long divertor legs, enabling measurements of the rotational temperature along the divertor leg.

Tables 1 and 2 summarise the MAST-U and TCV discharges examined in this paper. These generally either contain density ramp experiments (wide range of core densities, expressed as a fraction of the core Greenwald density, f_{GW} .) or experiments with as constant a range of core density as possible with divertor fuelling (narrow f_{GW} range). The configurations and fuelling locations referred to are shown in

Table 1. MAST-U discharges examined in this paper. The configurations ‘CD’, ‘ED’ and ‘SXD’ stand for Conventional Divertor, Elongated Divertor and Super-X Divertor respectively; and fuelling locations referenced can be seen in figure 2.

Discharge	Config.	Fuelling	Mode	$P_{\text{SOL}}^{\text{max}}$	f_{GW}	Isotope
49 408	CD	2	L	1.3 MW	0.25–0.50	D ₂
48 008	ED	2	L	1.3 MW	0.20–0.47	D ₂
48 358	SXD	2	L	1.3 MW	0.27–0.49	D ₂
49 286	SXD	2 + puffs: 3b, 3t	L	1.1 MW	0.25–0.32	D ₂
49 289	SXD	2, 3b, 3t	L	1.2 MW	0.25–0.37	D ₂
49 324	SXD	1, 3b, 3t	H	2.8 MW	0.49–0.596	D ₂

Table 2. TCV discharges examined in this paper. When two discharges are shown, they are repeat shots to enable full spectrometer coverage of the Fulcher band. The ‘CD’ configuration refers to a Conventional Divertor; and ‘SILO’ refers to Short Inner, Long Outer baffling. The fuelling locations can be referenced in figure 3 as can the baffling description.

Discharge	Config.	Fuelling	Mode	$P_{\text{SOL}}^{\text{max}}$	f_{GW}	Isotope
78 024/78 042	CD + SILO baffling	b	L	0.35 MW	0.18–0.54	D ₂
76 113/76 114	CD + no baffling	b	L	0.32 MW	0.18–0.57	D ₂
78 045	CD + SILO baffling	t	L	0.4 MW	0.19–0.54	D ₂
78 047	CD + SILO baffling	b	L	0.36 MW	0.2–0.44	D ₂
78 440/78 441	CD + SILO baffling	b	L	0.4 MW	0.2–0.49	H ₂

figures 2 and 3. The MAST-U discharges were beam-heated ($P_{\text{NBI}} > 1.5$ MW), while the TCV discharges were Ohmic. All the discharges were unseeded.

Figure 2 shows a schematic of the MAST-U tokamak device and indicates the three divertor configurations: Conventional (CD), Elongated (ED) and Super-X (SXD); the spectroscopic lines of sight in the upper divertor; and the fuelling locations relevant to the discharges examined in this paper. Adjacent lines of sight are separated by ~ 2.5 cm, and the spectra are acquired at 30 Hz.

Figure 3 shows a schematic of the TCV tokamak device in the conventional divertor (CD) configuration indicating the spectroscopic lines of sight and the fuelling locations relevant to the discharges examined in this paper. Adjacent lines of sight are separated by ~ 2 cm, and the spectra are acquired at 50 Hz.

In order to observe the evolution of the molecular rovibrational distribution with detachment, some meaningful measure of detachment is required. For this purpose, we adopt the peak ion target flux near the strike point (ions/m²/s) since it is observed that the rollover of the peak ion flux corresponds well to the separation of the Fulcher front (and therefore ionisation front) from the target [11]. Spectroscopic lines of sight near the strike point are selected for extracting the rovibrational information.

2.1. Spectroscopic analysis and extracting spectroscopic information

The rovibrational distribution is obtained using high resolution Fulcher band analysis using the technique described in detail in [13]. The rotational temperatures of D₂ and H₂ quoted in these results refer to the rotational temperature of the $\nu = 0$ band of the *ground* state. Rotational temperatures are obtained from the distribution of rotational energy levels in the

‘upper Fulcher state’, or $d^3\Pi_u^-$, experimentally observed via spectroscopic lines produced by spontaneous electronic decay from $d^3\Pi_u^-$ to $a^3\Sigma_g^+$. This Boltzmann distribution of rotational states is mapped to the ground state via a simple scale factor which relates the rotational temperature of the upper Fulcher state to the ground state.

Under conditions where the ground state is long-lived in comparison with characteristic collision time, then it is generally assumed that the rotational temperature of molecules in their electronic ground state can be used as a proxy for the kinetic, or ‘gas’, temperature within 10%–20% [33]. We find that the rotational states of the first vibrational band in the upper Fulcher state, a mapping of the distribution in the ground state, consistently form a good Boltzmann distribution in measurements. This suggests that collisionality is indeed high enough for equilibration between rotational and kinetic states.

Examples of spatial profiles of rotational temperature evolving during a discharge are shown in figure 4(a) for the MAST-U conventional, elongated and Super-X divertor configurations, and in figure 4(c) for the TCV conventional divertor configuration. The spectroscopic lines of sight in the MAST-U and TCV divertors are also shown in figure 4(b). The highlighted coloured blocks in both sets of diagrams show the groups of lines of sight near the strike-point. The rotational temperatures obtained at these locations are used to enable comparisons against multiple conditions/divertor shapes/devices.

Figures 5(a) and (b) show examples of imaging of the Fulcher emission in MAST-U and TCV corresponding to figures 4(a) (ED) and (c) respectively. The Fulcher emission front (an indicator of the ionisation front) is seen to detach from the target at around 500 ms in the MAST-U case, and after 1200 ms in the TCV case. These can be compared to peak particle flux (see figures 6(f) and (c) respectively) to observe the correlation with peak ion flux rollover).

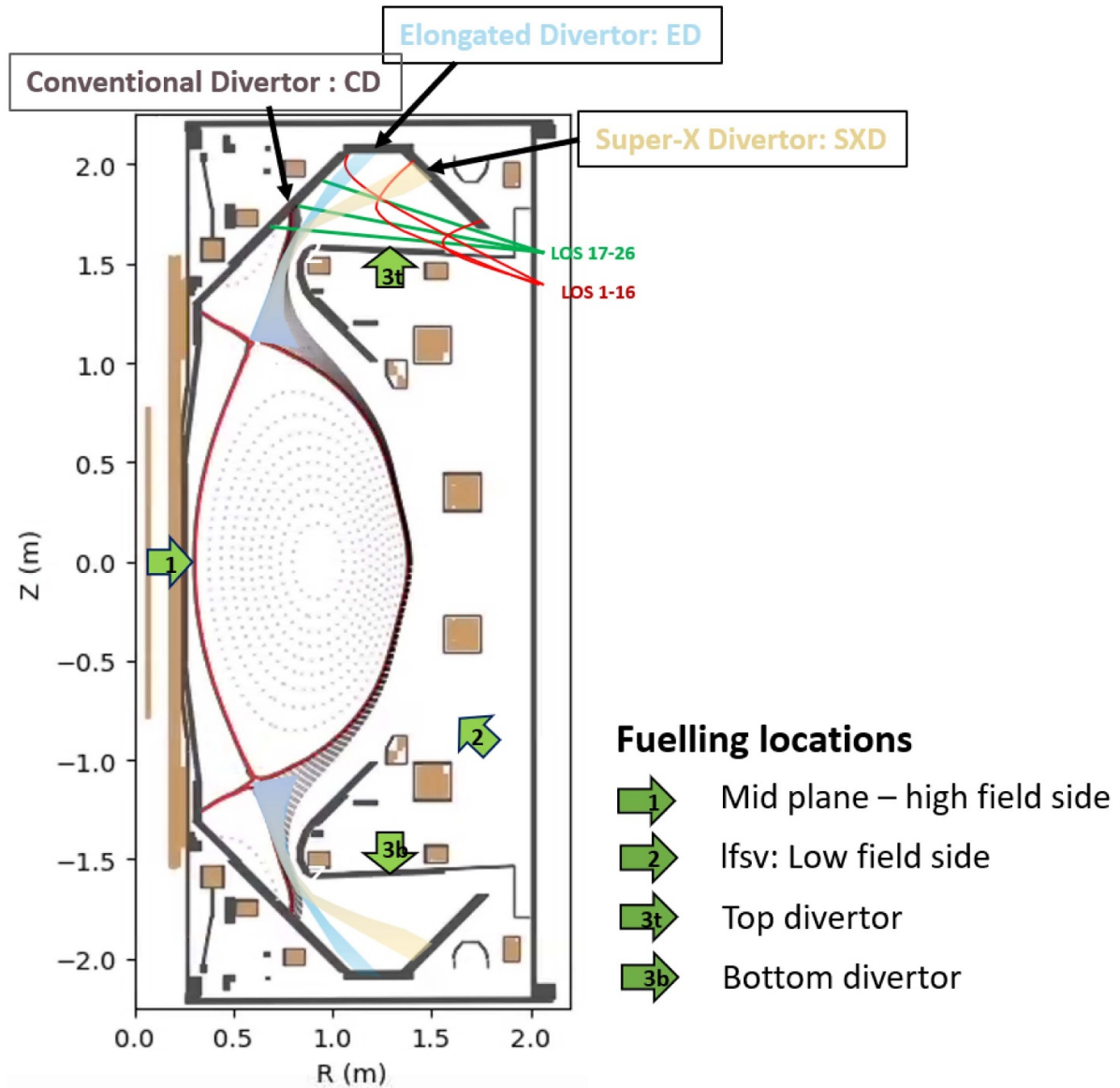


Figure 2. Schematic showing the divertor configurations, lines of sight and fuelling locations in the MAST-U upper divertor.

3. Results

3.1. Rotational temperature evolution at the strike point

Using variations in 1) divertor configuration (MAST-U); 2) neutral baffling (TCV); 3) fuelling location (TCV); 4) fuelling isotope (TCV) and 5) external heating levels (MAST-U) the rotational temperature near the strike point is investigated as function of core density. The core density is gradually increased using feed-back control to obtain density ramps.

Generally, we observe that the rotational temperature of the molecules rises as the core density is increased and the divertor is cooled (figure 6). The increase in rotational temperature occurs as the divertor nears detachment and increases during detachment, as can be seen from the saturation/decrease in ion target flux from where the graphs are shaded for ease

of reference (although some increase in rotational temperature can occur before detachment). At the deepest levels of detachment, a decay in rotational temperature is occasionally observed (MAST-U ED, SXD ($f_{GW} > 0.45$, figures 6(f) and (g))), which can be explained by the low plasma temperatures observed in these conditions ($T_e < 0.3$ eV estimated in [11]), according to our reduced model (section 4.1.1).

Remarkably, similar qualitative behaviour is observed for all 5 variations for both MAST-U and TCV. Although neutral baffling results in higher rotational temperatures at the same f_{GW} (figures 6(a) and (c)), it also reduces the detachment onset density: the rotational temperature increases as detachment is approached and becomes deeper in both cases. The same holds true for a change in fuelling location: divertor fuelling, as opposed to main chamber fuelling (to regulate the core density), reduces the detachment onset density and

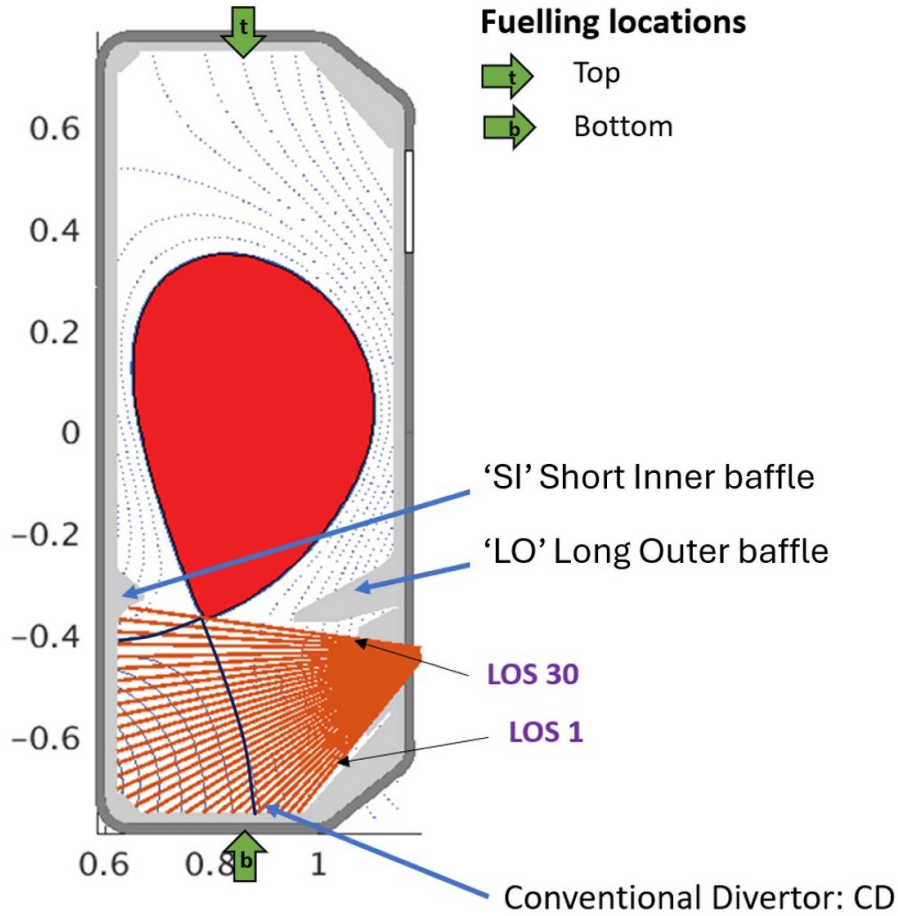


Figure 3. Schematic showing the divertor configuration, lines of sight and fuelling locations in the TCV divertor.

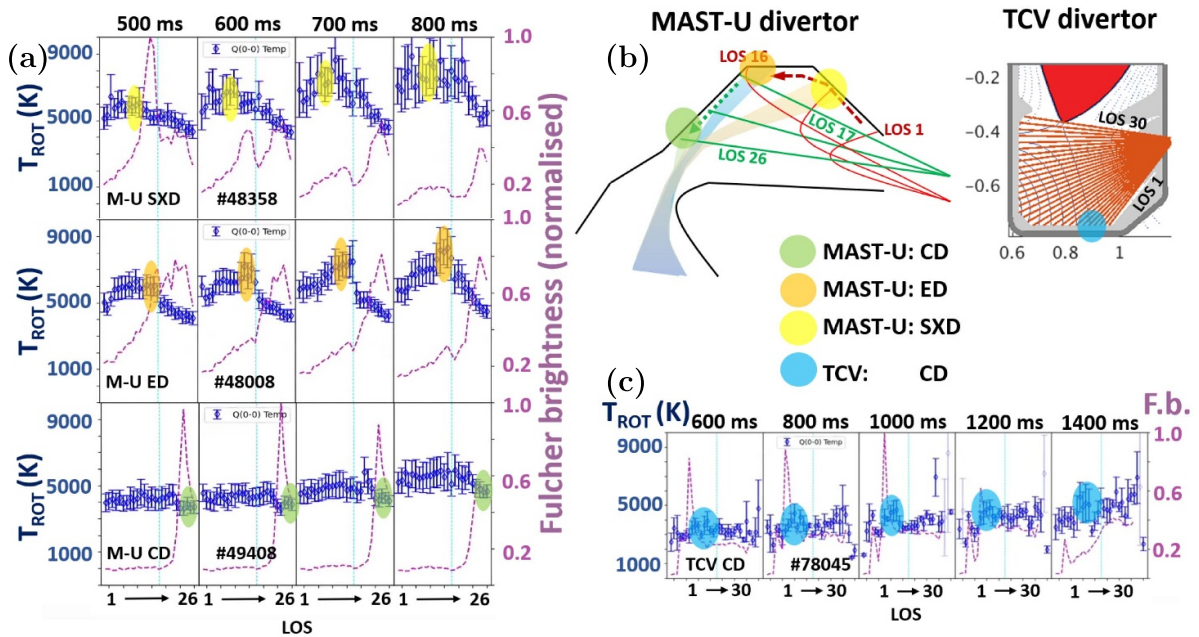


Figure 4. The areas of interest for each divertor configuration and imaging scans. The graphs in (a) show examples of the evolution of rotational temperature (T_{ROT}) across the divertor for an SXD, ED, and CD configuration in MAST-U. (c) Shows the evolution of T_{ROT} for TCV (CD configuration). (b) Shows the lines of sight (LOS) in the divertors of MAST-U and TCV and the highlighted colour circles indicate the grouping of LOS near the strike point in all configurations. These highlights correspond to the highlighted LOS in (a) and (c).

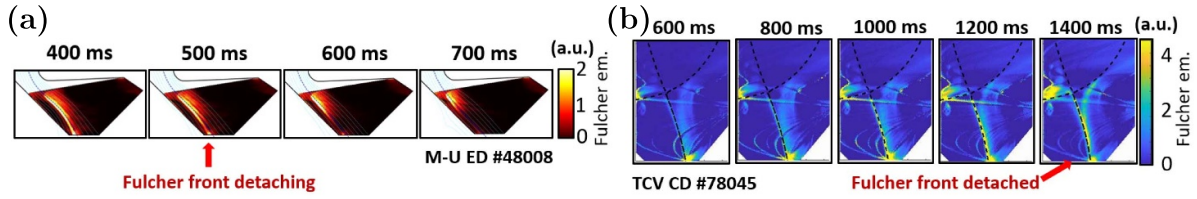


Figure 5. Fulcher emission imaging scans at various times during (a) the ED MAST-U discharge 48 008 and (b) the TCV discharge 78 045. (Note in (b) inspection of camera footage reveals that the bright spot seen at the target after detachment is likely due to impurity radiation.)

increases the depth of detachment, leading to higher rotational temperatures (figures 6(b) and (c)). Similar results were also obtained in MAST-U Ohmic conditions [13], indicating that this qualitative behaviour (at the same level of detachment) is mostly independent of the level of heating applied. Even with H_2 ($\sim 80\%$), as opposed to D_2 , similar behaviour is observed (figures 6(c) and (d)).

There are quantitative differences between the different cases, however. The rotational temperatures obtained for H_2 are lower than for D_2 . The rotational temperatures obtained on MAST-U, as well as the range of its increase, are generally higher than on TCV. This may be associated with the strong baffling on MAST-U.

Figure 7(a) shows a TCV discharge in which the core density was held constant after an initial ramp. We see that the rotational temperature increases and then holds roughly level with the core density indicating that divertor conditions hold steady with core density in such Ohmic discharges.

In MAST-U H-mode (higher heating power), where core density is kept constant, and divertor neutral pressure is increased through divertor fuelling (figure 7(b)), a high rotational temperature with some increase is observed in keeping with the degree of detachment.

To obtain a clearer picture of the impact of divertor fuelling (room temperature D_2 from valve 3t (see figure 2)) on plasma-molecular kinetics and detachment, two additional MAST-U experiments (beam-heated L-mode) are performed. Both discharges are detached before divertor fuelling is introduced. During discharge 49 286, two sharp D_2 puffs were injected into the upper divertor from valve 3t (see figure 2) at 400 ms and 600 ms (and two puffs into the lower divertor at 500 ms and 700 ms). Discharge 49 289 experienced a fuelling ramp, symmetric between lower and upper divertor.

For both cases, an increase in rotational temperature (far beyond room temperature) is observed during room temperature D_2 gas injection in the divertor (figure 8). The additional divertor cooling/deeper detachment induced by divertor fuelling (as evidenced by a reduction in ion target flux) results in an increase in rotational temperature. This observation is the most clear in the case where two sharp divertor puffs are introduced (figure 8(a)), corresponding to an immediate reduction in ion flux and surge in rotational temperature, after which the ion flux and rotational temperature recovers until the second puff is introduced. Additionally, the upper divertor neutral pressure and rotational temperature do not respond to the staggered lower divertor puffs (at 500 ms and 700 ms) suggesting a decoupling between

lower and upper divertor. This is in keeping with finding by Kool *et al* [14].

To conclude, the rotational temperature rises throughout the detachment process. The increase tends to be more pronounced when particle flux ‘rolls over’ and the plasma becomes deeply detached.

3.2. Vibrational distribution

Using D_2 Fulcher emission, the vibrational distribution of the first four vibrational bands (in the Fulcher state— $d^3\Pi_u$) is measured at the strike point location. The vibrational distribution determines, to a large extent, the chemical interactions that the molecules can undergo with the plasma that result in the formation of molecular ions that lead to MAR and MAD.

The vibrational distribution changes after detachment onset (figures 9 and 10) for a range of MAST-U and TCV conditions. This is consistent with previous MAST-U Ohmic observations [13] where a correlation between the rotational temperature and an elevation of the $\nu = 2, 3$ Fulcher bands was observed. Such an elevation is in disagreement with a Boltzmann distribution in the ground state, mapped to the upper Fulcher state; the vibrational distribution cannot be quantified with a vibrational temperature.

To estimate the populations of the vibrational bands, we use rotational lines which occur unimpeded in the $\nu = 0$ band and in at least one more to build a composite plot with as much information as possible that can then be averaged. The full technique is described in the appendix of [13]. In MAST-U experiments, this was possible in one single discharge since the ‘DIBS’ spectrometer (Divertor Imaging Balmer Spectrometer) has sufficient coverage (595–626 nm) to capture all four bands at high resolution (0.04 nm) [13]. However, in TCV experiments, a repeat discharge was required to capture the information.

In cases where detachment does not occur (or is very weak) (figures 6(a) and (e)) the vibrational distribution (relative to $\nu = 0$ in the Fulcher state) changes negligibly (figures 9(a) MAST-U, CD; (b) TCV, unbaffled). This is in contrast to the strongly detached TCV baffled and MAST-U SXD discharges, where a clear change in the vibrational distribution during the core density ramp is observed. To allow ease of reference, these two different density ranges have been separated in figure 10. The vibrational distribution starts to change near (TCV) or after (MAST-U) the detachment onset (figures 6(b) and (g) respectively) and becomes larger as detachment progresses.

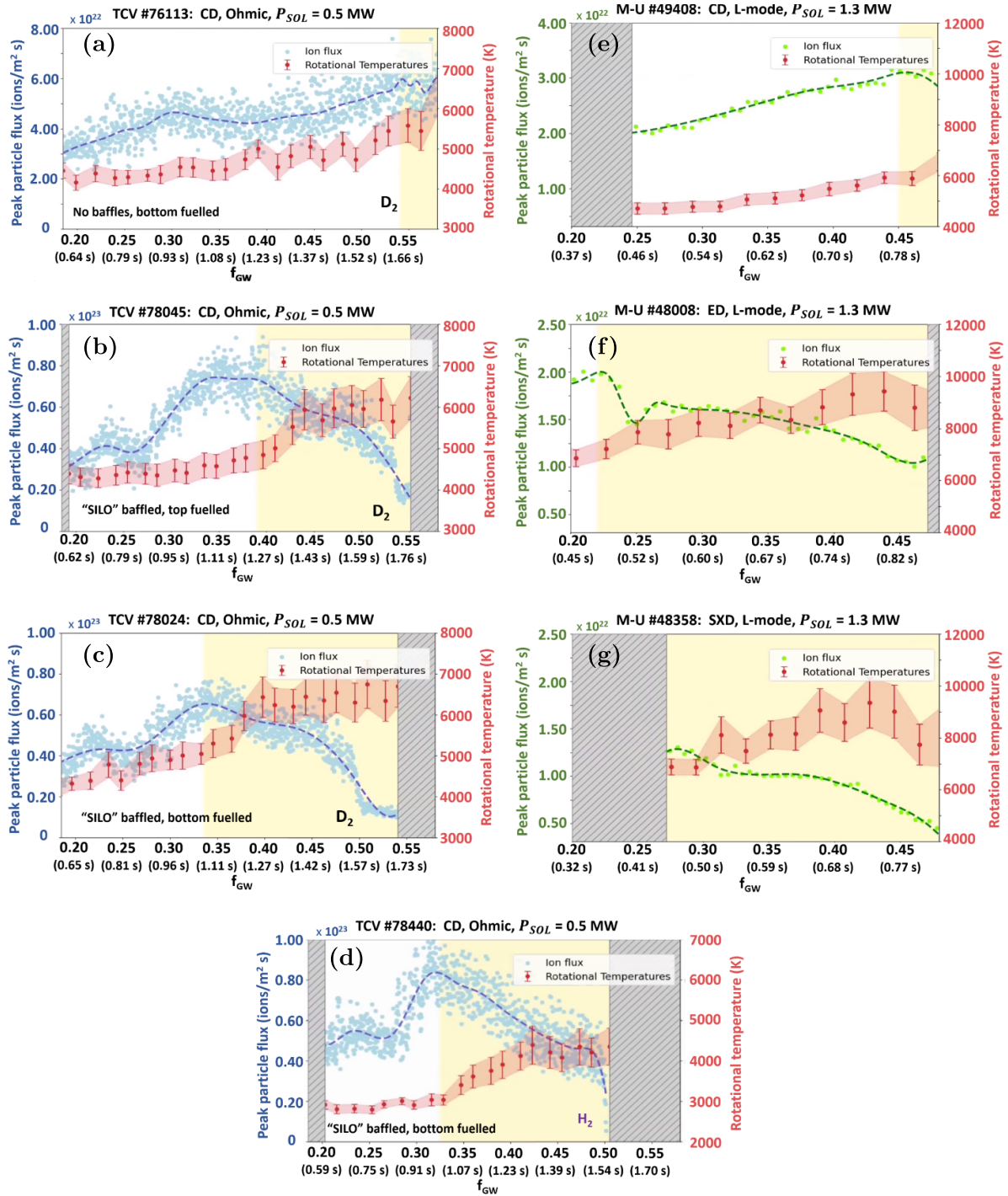


Figure 6. Graphs showing the evolution of rotational temperature at the strike point in several density ramps. Plots (a)–(d) show Ohmic density ramps for TCV (note that (d) is an isotopic variation). Meanwhile, plots (e)–(g) show CD, ED and SXD beam-heated L-mode discharges for MAST-U. Note the different temperature scales. Both Greenwald fraction and time are indicated on the x-axis. The lemon-coloured shading indicates the transition to detachment.

4. Discussion

We have the following two principal observations from the experimental results:

- The rotational temperature of the molecules in the divertor is seen to rise during the detachment process, even when the introduction of *cold* molecules in the divertor further deepens detachment.

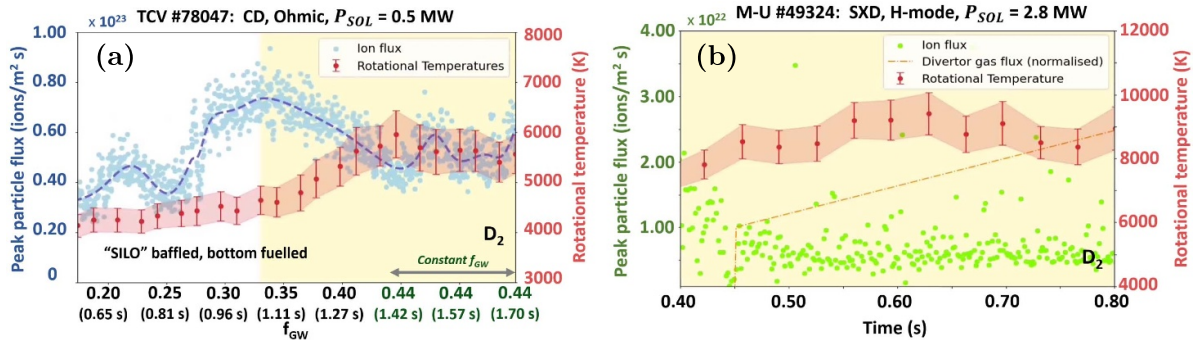


Figure 7. Graphs showing the evolution of rotational temperature at the strike point in: (a) a TCV discharge with core density held constant from 1.4 s after initial ramp; (b) H-mode fuelling scan MAST-U.

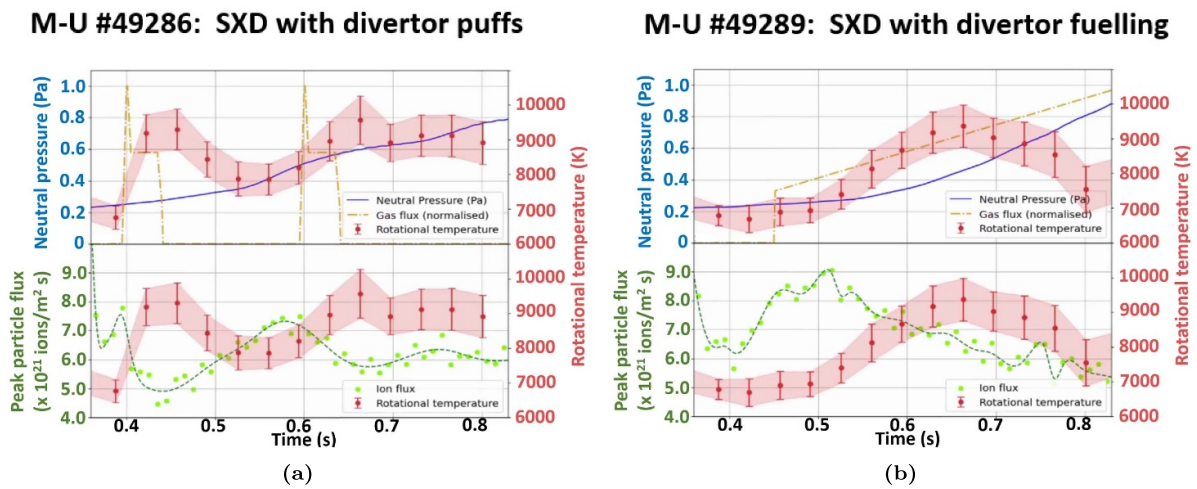


Figure 8. MAST-U discharges with divertor fuelling from valve 3t (see figure 2). The top plots show the divertor D₂ gas flux and the neutral pressure; and the lower plots show the peak particle flux at the strike point. The rotational temperature near the strike point is shown in both cases for reference. (a) Shows 49 286 in which two sharp puffs of D₂ were injected at 400 ms and 600 ms. (b) Shows 49 289 during which there is a fuelling ramp.

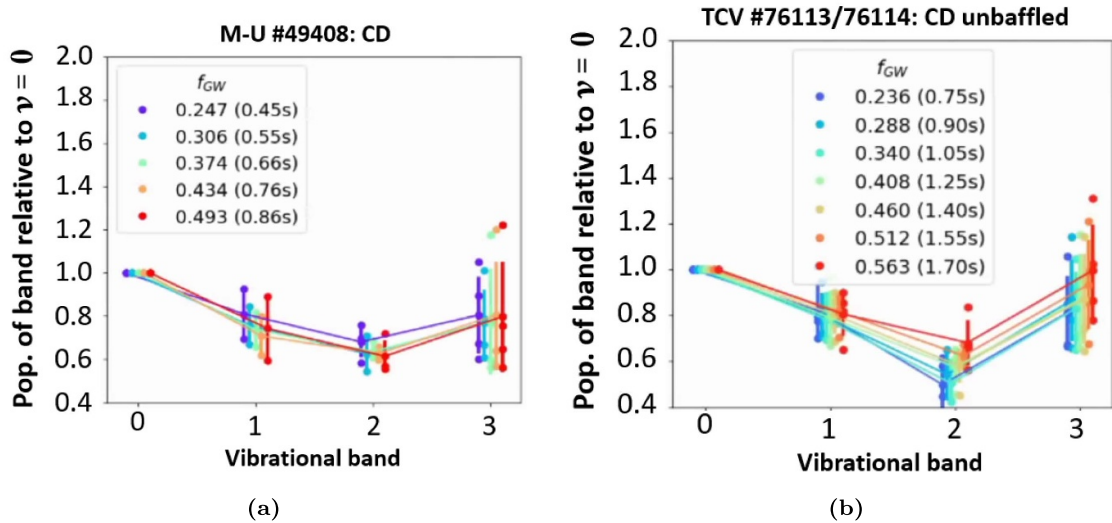


Figure 9. The evolution of the vibrational distributions of bands $\nu = 0, 1, 2, 3$ for (a), a CD MAST-U density ramp, and (b), an unbaffled TCV density ramp.

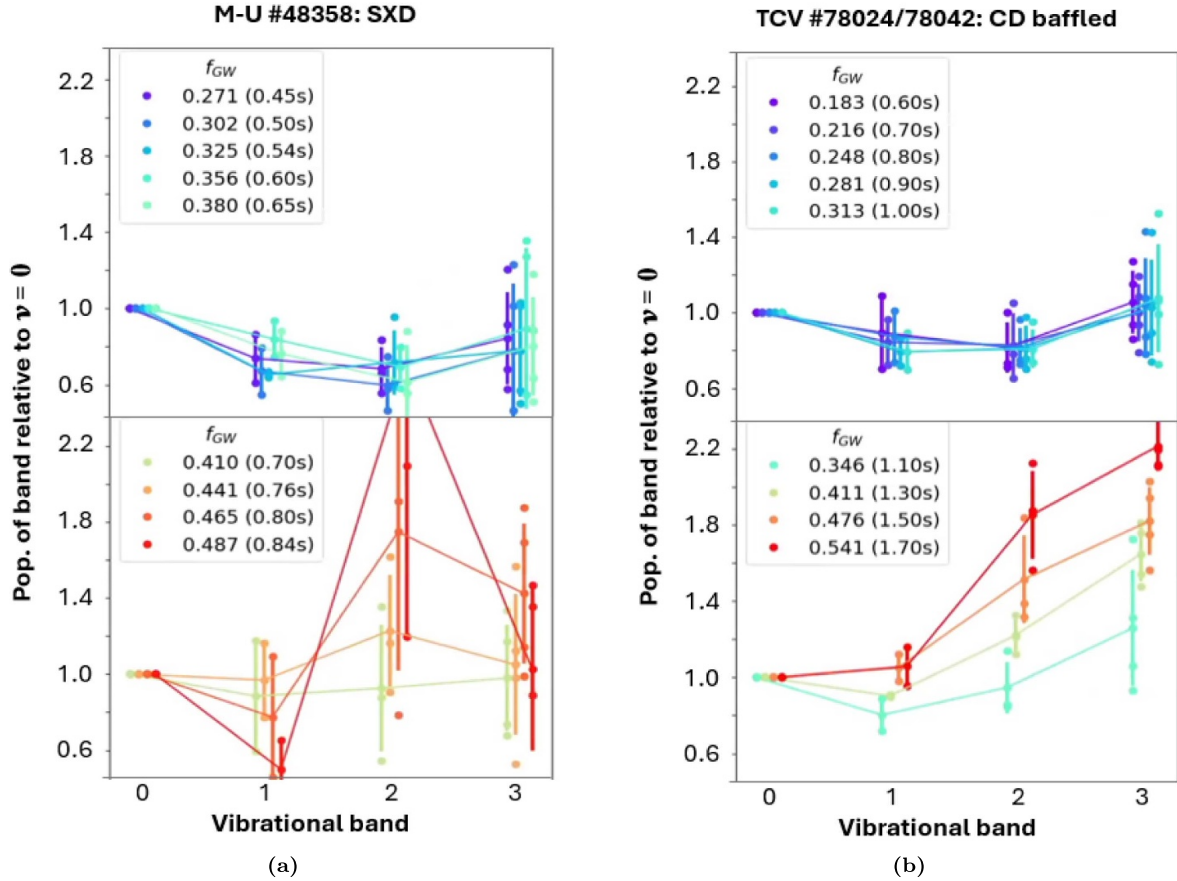


Figure 10. Graphs showing the vibrational distribution of the first four vibrational bands for an SXD density ramp MAST-U (a) and baffled density ramp TCV (b). The populations of bands $\nu = 1, 2, 3$ are shown relative to $\nu = 0$. The top and bottom graphs in each subfigure show the distribution before and after a population boost occurs for $\nu = 2, 3$.

- Deepening of detachment results in a change of vibrational distribution in both MAST-U and TCV, which cannot be quantified with a Boltzmann distribution and a vibrational temperature in the ground state [13].

4.1. Understanding the increased gas temperature during detachment

As was discussed earlier, the rotational temperature of the molecules in the ground state of the first vibrational band, is often taken as a proxy for the D_2 gas temperature [33]. We aim to explain why this gas temperature increases during detachment using a reduced model and exhaust modelling comparisons.

4.1.1. Reduced model for molecular gas temperature. To explain the increase in rotational, or ‘gas’ temperature, we imagine a reduced model describing neutrals (D and D_2) in a bath of D^+ ions at temperature T_i undergoing elastic collisions with the ions.

This reduced model is based on the following assumptions/principles, resulting in the conclusion that energy transfer from the ions to the molecules is more efficient at lower plasma temperatures, when the lifetime of the molecules in the divertor is increased.

- The dominant energy transfer mechanism from the plasma to the molecules is assumed to be ion-molecule elastic collisions.
- The temperature reached by the molecules via this mechanism is limited by their lifetime in the region of interest, which ends when they are either destroyed through a plasma reaction, or transported out of the region.

We can calculate how the temperature T of the D_2 molecules evolves over time by considering the energy entering and exiting the molecular cloud in the plasma leg. This leads to the following differential equation for the gas temperature (derived in the appendix):

$$\frac{dT}{dt} \approx 0.4 n_i \sigma_{\text{rep}} \left[\frac{k(T + 2T_i)}{m_i} \right]^{\frac{1}{2}} (fT_i - T) - \frac{T}{\tau_{\text{eff}}} + \frac{T_{\text{wall}}}{\tau_{\text{eff}}}. \quad (22)$$

In equation (22), the first term on the right-hand-side originates from energy being transferred to the molecular cloud due to ion-molecule elastic collisions, the second term on the right-hand-side accounts for losses due to either destruction or transport, and the third term replaces lost molecules at the wall temperature to conserve molecular density. n_i is the ion density, and σ_{rep} is a representative cross-section for elastic

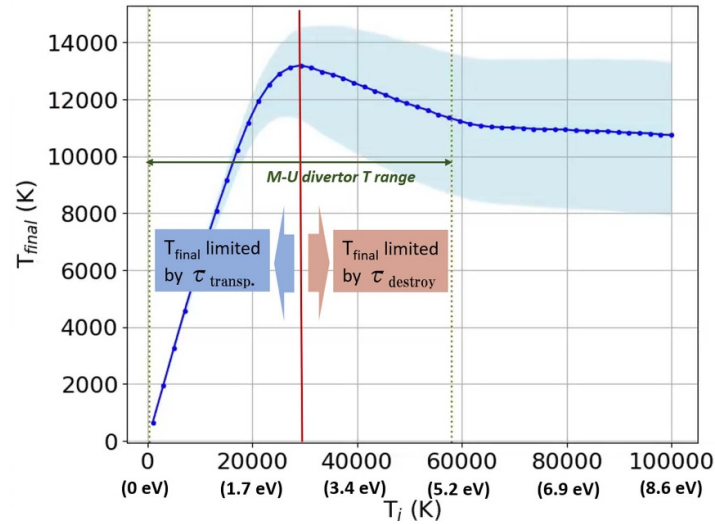


Figure 11. The final molecular temperatures achieved in the simplified model for a complete scan of ion-bath temperatures. $n_i = 2 \times 10^{19} \text{ m}^{-3}$. The shaded region allows for uncertainty in σ of 30%. The dotted green vertical lines indicate the range of divertor temperatures in the MAST-U divertor during a typical SXD discharge.

collisions between ions and molecules at a given temperature extracted from the Amjuel Eirene database [34] — see appendix). f is an efficiency term to account for exchanged energy which does not end up in the translational or rotational energy of the molecules. The most likely source of this inefficiency is energy causing vibrational excitation. f would be likely to increase with ion temperature as vibrational excitation becomes more probable. τ_{eff} encapsulates both the characteristic destruction time τ_{dest} and transit time τ_{transp}

$$\frac{1}{\tau_{\text{eff}}} = \frac{1}{\tau_{\text{dest}}} + \frac{1}{\tau_{\text{transp}}}. \quad (1)$$

To calculate τ_{dest} , the following destruction mechanisms are considered: molecular ionisation $e + \text{D}_2 \rightarrow 2e + \text{D}_2^+$; electron-impact dissociation $e^- + \text{D}_2 \rightarrow e^- + \text{D} + \text{D}$; and molecular charge-exchange $\text{D}^+ + \text{D}_2 \rightarrow \text{D} + \text{D}_2^+$. Rates for these reactions are sensitive to plasma temperature and electron density [34]

$$\frac{1}{\tau_{\text{dest}}} = n_e \langle \sigma v \rangle_{\text{ionisation}} + n_e \langle \sigma v \rangle_{\text{dissociation}} + n_e \langle \sigma v \rangle_{\text{CX}}. \quad (2)$$

In the model, we assume $T_i = T_e$ and $n_e = n_i$. τ_{dest} is primarily driven by electron-impact dissociation in attached conditions ($T_e > 5 \text{ eV}$). Typically τ_{dest} may range from $\mathcal{O}(1 \text{ s})$ in a cold 0.1 eV plasma to $\mathcal{O}(1 \text{ } \mu\text{s})$ in a hot 20 eV plasma.

The transport time τ_{transp} limits the transit time of a molecule across the divertor (e.g. plasma) leg. It is calculated assuming a simple 1D random walk (see appendix for further details). Typical values for τ_{transp} across the MAST-U divertor leg are $\mathcal{O}(100 \text{ } \mu\text{s})$.

In this way the characteristic destruction time τ_{dest} will dominate ($\tau_{\text{dest}} \ll \tau_{\text{transp}}$) in a hot plasma while the characteristic transport time τ_{transp} dominates ($\tau_{\text{transp}} \ll \tau_{\text{dest}}$) in a cold plasma. The cross-over is at around 2–3 eV.

For a given ion temperature, while σ_{rep} varies as T evolves, this variation is very small. If we also take a characteristic

τ_{transp} such that we neglect its variation with T , and use the approximation $T \ll T_i$, we can write down an approximate equilibrium ($\frac{dT}{dt} = 0$) analytical solution for equation (22):

$$T \approx \frac{0.4fn_i\sigma_{\text{rep}}v_{\text{th}}T_i + \frac{T_{\text{wall}}}{\tau_{\text{eff}}}}{\frac{1}{\tau_{\text{eff}}} + 0.4n_i\sigma_{\text{rep}}v_{\text{th}}}, \quad (3)$$

where $v_{\text{th}} = \sqrt{2kT_i/m_i}$.

From this solution, using MAST-U relevant parameters, and assuming an energy exchange efficiency of $f = 0.75$, we obtain figure 11 showing the equilibrium gas temperature for various ion temperatures, taking into account the lifetime of the molecules due to plasma reactions, and their transit time through the plasma leg.

The highest gas temperature is reached at moderate ion temperatures of a few eV—cold enough to provide relatively long molecular lifetimes, but energetic enough to heat up the molecule within its transit time. This is qualitatively consistent with the observation that the rotational temperature increases during detachment: the gas temperature increases because the molecules live longer and undergo more collisions with the plasma. Introducing fuelling into a detached divertor leads to deeper detachment and longer molecular lifetimes, increasing the gas temperature obtained. A decay of rotational temperature is observed in the deepest detached conditions (figures 6(f) and (g)), where the plasma is insufficiently energetic to heat up the molecules (within their transit times), in agreement with the model. The range of gas temperatures obtained by the model are in reasonable quantitative agreement with the MAST-U measurements. We note also that, according to the model, lighter molecules would have shorter transport times and therefore achieve lower temperatures which is consistent with the TCX isotope study comparing H_2 and D_2 (figures 6(c) and (d)).

This model is intended to capture key physics in a (semi-)classical approach, and complications are avoided

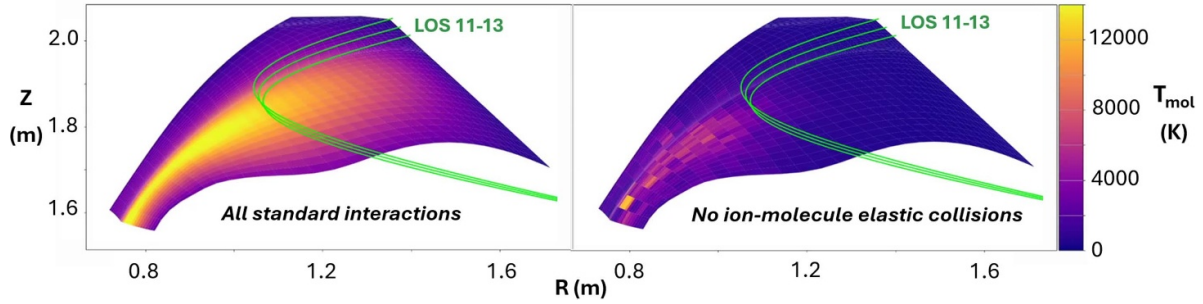


Figure 12. The molecular temperature generated by SOLPS-ITER (1 MW detached SXD) for all standard reactions (left plot), and all reactions *except* ion-molecule elastic collisions (right plot).

where reasonably possible. We, therefore, note the following limitations of our model:

- The use of a representative constant density.
- The use of a constant cross-section in the energy exchange rate from [35]. This is addressed by selecting an appropriate representative value (see [appendix](#)) and allowing for a generous uncertainty.
- Neglecting other energy transfer pathways, in particular vibrational excitation. This is addressed by incorporating an efficiency factor f in the energy exchange term.
- Neglecting surface effects. Our model replaces molecules at the wall temperature. It should be noted, however, that research points to the significance of recycling with regard to rovibrational excitation via mechanisms such as Eley-Rideal (ER) [19–21, 36]. Some preliminary work by [37] suggests significant changes to the vibrational distribution and possible increases in molecular temperature of up to 20%–30% after the onset of detachment when the ER mechanism is switched on in MAST-U SOLPS-ITER simulations.
- Not evolving the ion temperature. This may marginally inflate the molecular temperature reached.
- Not accounting for electron temperature effects. Elastic collisions with electrons were investigated and our modelling suggests that in relevant divertor conditions, the electrons supply less than 10% of the energy required to explain the increase in temperature.

It does not treat the various rovibronic transitions that could result in rotational excitation. Such processes have been considered in collisional-radiative models, where it was suggested that electron collisions can have a significant impact on the rotational distribution, particularly in high temperature conditions ($T_e \sim 10$ eV) [26].

4.1.2. Comparison against molecular gas temperature in SOLPS-ITER simulations. Using interpretive exhaust simulations by Moulton *et al* we compare the molecular gas temperatures obtained against experiments and investigate the mechanisms resulting in an increase in molecular gas temperature. The simulations were fuelled from the low field side in keeping with the MAST-U experiments, and had no drifts

(there is little vertical asymmetry expected at 1 MW). The simulations are otherwise similar to those described in detail in [38] but with 1 MW input power.

The molecular gas temperature obtained from exhaust simulations is compared for a default rate setup and a modified setup where the only change is the disabling of elastic collisions between ions and molecules (figure 12). This shows: 1) the molecular temperature obtained is significantly higher than the ‘cold’ gas injected and is in a similar range as the (rotational) temperatures observed on MAST-U; and 2) the molecular temperature is primarily driven by elastic ion-molecule collisions. Additionally, a decrease in molecular temperature near the target is observed, consistent with our reduced model (figure 11) and experiments at deepest detachment (figure 8(b)). This provides additional evidence that ion-molecule collisions are dominant in the energy transfer from the plasma to the molecules. (It is worth noting that the remaining high temperatures in the right-hand-side plot of figure 12 are due to atom-molecule collisions, and that the molecular temperature flattens completely if these are also disabled).

To enable a quantitative comparison between experiments and simulations, a synthetic diagnostic setup is used. Here, the Fulcher-emission weighted averaged D_2 temperature, along a spectroscopic line-of-sight is obtained. Since D_2 Fulcher emission is used to infer the rotational temperature, the rotational temperature estimate corresponds to the region along the line-of-sight where emission occurs.

We compare an SXD density ramp (discharge 48358) against a sequence of simulations for an SXD configuration with very similar geometry. Figure 13 shows the result. The correspondence is made via the fuelling rate (blue line) - but some caution is needed noting that, although the fuelling location is the same in both cases, there is considerable uncertainty in the fuelling rate experimentally speaking. We also note that the input power is 1 MW in the simulations, but has considerable uncertainty in the experimental discharge (1.3 ± 0.2 MW). Despite these caveats, the synthetically obtained molecular temperatures in the SXD simulations have a range similar to the rotational temperatures experimentally observed. The increase in temperature with detachment is also in reasonable agreement.

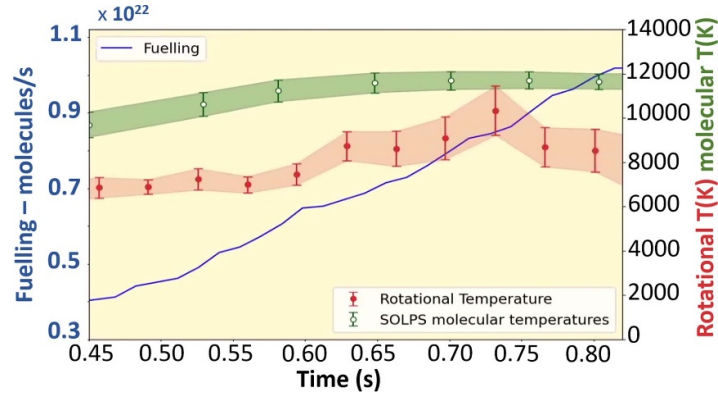


Figure 13. The red plot shows the experimentally determined rotational temperatures averaged across a group of LOS (11-13 shown on figure 12) at various degrees of detachment. The green plot shows the SOLPS inferred molecular temperatures from several different simulations for the same LOS grouping. The simulations are matched to the experiment via the fuelling rate (blue line).

4.2. Vibrational distribution

To obtain further insight into the expected vibrational distribution in the D_2 Fulcher state, the vibrational distribution in the electronic ground state ($X^1\Sigma_g$) is modelled using a collisional-radiative model setup [16] that mimics the Eirene vibrationally resolved setup (H2vibr) [39] with corrected molecular charge exchange rates [40] using the CRUMPET [41] framework (see [16, 42] for more details). With this, we can model the $X^1\Sigma_g$ vibrational distribution that was implicitly assumed in the derivation of the rates employed by Eirene. Franck-Condon coefficients [27, 28] are used to map the $X^1\Sigma_g$ vibrational distribution to the D_2 Fulcher state ($d^3\Pi_u$), using the approach highlighted in [13]. It should be noted that both a setup identical to Eirene and a modified setup with corrected molecular charge exchange rates (both presented in [16]) were used for this study and resulted in the same interpretation.

With this approach, we can compute the $d^3\Pi_u\nu = 1, 2, 3$ distribution, relative to $d^3\Pi_u\nu = 0$, as a function of T_e (which is assumed to be equal to the ion temperature; a reasonable approximation according to SOLPS-ITER simulations). According to the modelled distribution, an increase in the $d^3\Pi_u\nu = 2, 3$ states is expected for $T < 1.3$ eV (figure 14(b)), which seems to be qualitatively consistent with the experimentally observed change during detachment (figure 10). Comparing the modelled distributions in the $X^1\Sigma_g$ and $d^3\Pi_u\nu = 1, 2, 3$ states suggests that this increase in the upper Fulcher state corresponds to a reduction in population of the high vibrational levels in the electronic ground state. This reduction in the ground state distribution occurs due to the electron temperature becoming insufficient to drive vibrational excitation, and the depletion of highly vibrationally excited molecules through MAR and MAD. The surprising correspondence to *increased* populations in the upper Fulcher state comes about because of the non-trivial way in which the ground state distribution maps to it using Franck-Condon factors.

However, we note two disagreements with the experiment: 1) $d^3\Pi_u\nu = 1, 2, 3$, with respect to $d^3\Pi_u\nu = 0$, is expected to decrease from > 5 eV to lower temperatures

(before detachment) in the modelled distribution. However, no changes in the vibrational distribution are observed. This may be explained by the omission of vibrational excitation through electronic excitation followed by radiative decay (e.g. $e^- + D_2(\nu_1) \rightarrow e^- + D_2^*$, $D_2^* \rightarrow \gamma + D_2(\nu_2)$). This under-predicts vibrational excitation above 1.5 eV [18, 42], resulting in a decrease in vibrational excitation above 1.5 eV, which does not occur if such reactions are included in the CRM [42].

A second disagreement is the observation that $d^3\Pi_u\nu = 1$ increases together with $d^3\Pi_u\nu = 2, 3$ for $T < 1$ eV in the modelled distribution, which does not occur experimentally. The cause of this is unclear. It is known that recycling mechanisms such as ER and Langmuir–Hinshelwood can affect the vibrational distribution [19–21, 36]. Potentially, such interactions in combination with transport of vibrationally excited molecules could result in a reduced temperature sensitivity for the $d^3\Pi_u\nu = 1$ state, or other changes, requiring further study.

We note that there are large uncertainties in the vibrational distribution measurements at the lower signals at lower temperatures (see figure 10) making these discrepancies of a qualitative nature.

4.3. Power and momentum losses from elastic plasma-molecule collisions

Elastic collisions between the ions and the molecules, resulting in a molecular ‘gas’ temperature increase that is observed, are also accompanied with significant plasma power and volumetric momentum losses according to SOLPS-ITER simulations, playing a significant role in detachment [15, 43].

Reduced models focussing on the neutral buffer during detachment have been proposed in the past to study volumetric momentum losses from plasma-atom interactions [44, 45], as well as for the energy required to ionise (burn through) the neutral buffer with regard to transients [46].

In this section, we use ‘back-of-the-envelope arguments’, in combination with rotational temperature observations and other experimental measurements (ionisation front position, neutral pressure) to experimentally estimate power and

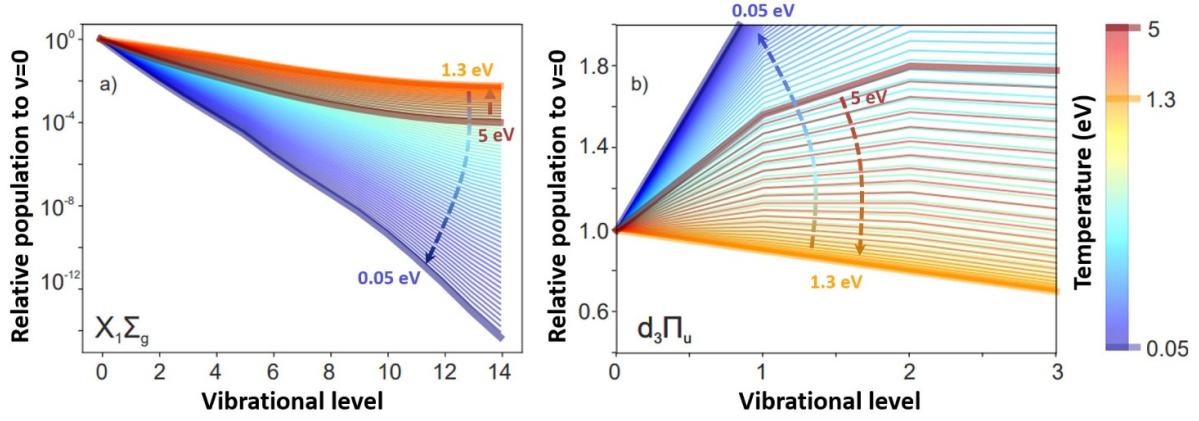


Figure 14. Vibrational distribution in the electronic ground state (a, $X_1\Sigma_g$) and upper Fulcher state (b, $d_3\Pi_u$), relative to the $\nu = 0$ population (for the respective electronic state) for different temperatures ranging from 5 eV to 0.05 eV according to an ‘Eirene-like’ CRM setup. The distribution in the upper Fulcher state is obtained through mapping the ground state distribution using a Franck-Condon approach.

momentum losses from elastic ion-molecule collisions, which are compared against SOLPS-ITER simulations.

4.3.1. Experimental power loss estimates from elastic plasma-molecule collisions with modelling comparison. Assuming the rotational temperature is a proxy for the gas temperature, our rotational temperature measurements can be used as a proxy for these plasma power losses. To achieve this, we make a simplified estimate of the power losses obtained experimentally. First, the power transfer per molecule should be estimated. Assuming the molecules heat up from room temperature to the observed rotational temperature within their transit time, the power transfer per molecule can be estimated as

$$P_{\text{mol}}^1 = \frac{5k\Delta T_{\text{rot}}}{2\tau_{\text{transport}}}, \quad (4)$$

where $\Delta T_{\text{rot}} = T_{\text{rot}} - T_{\text{wall}} \approx T_{\text{rot}}$.

To obtain the total energy loss, this should be multiplied with the total amount of molecules in the system, which depends on the molecular density (n_{mol}) and the volume of the neutral gas buffer (V)

$$P_{\text{mol}} = P_{\text{mol}}^1 \times n_{\text{mol}} \times V. \quad (5)$$

The molecular density can be estimated from the measured divertor neutral pressure $p_n = n_n^{\text{gauge}} k T_{\text{gauge}}$, where n_n^{gauge} is the neutral density at the gauge. This is measured by the fast-ion gauge in the sub-divertor beyond the wall. We use a molecular flow model, with conservation of flux, to simulate a synthetic baratron (as previously done in [47, 48]) to account for the various pipework in between the fast-ion gauge and the tokamak to link the molecular density in the divertor to the molecular density at the gauge:

$$n_{\text{mol}}^{\text{div}} \approx n_{\text{mol}}^{\text{gauge}} \sqrt{\frac{T_{\text{gauge}}}{T_{\text{mol}}}}. \quad (6)$$

Assuming that, in the sub-divertor, the molecules dominate the neutrals, such that $n_n^{\text{gauge}} = n_{\text{mol}}^{\text{gauge}}$; and further assuming that

the gauge operates at the wall temperature ($T_{\text{gauge}} = T_{\text{wall}}$), and that $T_{\text{mol}} = T_{\text{rot}}$, we arrive at:

$$n_{\text{mol}}^{\text{div}} = \frac{p_n}{k\sqrt{T_{\text{wall}}T_{\text{rot}}}}. \quad (7)$$

It is assumed that the molecular density is constant throughout the neutral gas buffer.

The neutral gas buffer is assumed to exist only downstream the ionisation front. The poloidal distance between the target and the ionisation front is denoted as L_{pol} and is obtained using the D_2 Fulcher emission front as a proxy for the ionisation front [11–13]. The volume of the neutral buffer is then $2\pi R L_{\text{pol}} w$, where w is the width of the divertor leg and R is the radius of the divertor leg.

Taking the various components together, combined with $\tau_{\text{transport}} = \frac{w}{v_{\text{eff}}}$, the power loss can be approximated as suggested in equation (8)

$$P_{\text{mol}} \approx 5\pi v_{\text{eff}} \sqrt{\frac{T_{\text{rot}}}{T_{\text{wall}}}} L_{\text{pol}} p_n R. \quad (8)$$

This provides an intuitive model for power losses from plasma-molecular collisions, which start after the detachment onset ($L_{\text{pol}} > 0$ m) and are driven by: 1) rotational temperature; 2) detachment front position; 3) divertor neutral pressure.

The model can be made more accurate by accounting for spatial variations of T_{rot} in the divertor. Since T_{rot} is experimentally obtained along a spectroscopic line of sight, chord-integrated power loss estimates can be obtained along each line of sight $P_{\text{mol}}^{\text{LoS}} [\text{W m}^{-2}]$, which can be integrated toroidally (e.g. $2\pi R$ along the curve where the lines of sight intersect the separatrix, up to the ionisation front a distance L_{pol} from the target) to obtain the total power loss, analogously to how ion sources and sinks are obtained experimentally [4]

$$P_{\text{mol}} = 2\pi \int_0^{L_{\text{pol}}} R(s) P_{\text{mol}}^{\text{LoS}}(s) ds$$

$$P_{\text{mol}}^{\text{LoS}}(s) \approx \frac{5p_n v_{\text{eff}}(s) \sqrt{T_{\text{rot}}(s)}}{2\sqrt{T_{\text{wall}}}}. \quad (9)$$

The estimated total power losses from plasma-molecular collisions in both divertors, according to this estimate, are significant for the Super-X divertor and increase as the core density is increased due to: 1) a movement of the ionisation front further upstream; 2) increase in divertor neutral pressure; 3) increase in rotational temperature observed.

To apply this for MAST-U SXD discharge 48 358 (see figure 15), we utilise our rotational temperature and neutral pressure divertor measurements. The approximate variation of L_{pol} with f_{GW} in a MAST-U beam-heated density ramp is taken from [49] (a repeat discharge of 48 358) and we find a range $L_{\text{pol}} \approx 36 - 52$ cm corresponding to $f_{\text{GW}} \approx 0.30 - 0.46$.

To calculate v_{eff} :

$$v_{\text{eff}} = \frac{\langle v_{\text{th}} \rangle}{\sqrt{2}wn\sigma} \quad \text{where} \quad \langle v_{\text{th}} \rangle \approx \sqrt{\frac{4k_b T_{\text{rot}}}{3m_{D_2}}} \quad (\text{see appendix}), \quad (10)$$

we require several other parameters as well as the T_{rot} measurements. The cross-section is taken as $\sigma \approx 6.5 \times 10^{-19} \text{ m}^2$ from the AMJUEL data file 1.2.7 [34] (along with an appropriate scaling). We take an approximate ion divertor density appropriate for calculating the mean free path of the molecules: $n_i \approx 2 \times 10^{19} \text{ m}^{-3}$ (see [50]), T_{wall} is taken as 300 K, and the width of the plasma leg (based on poloidal flux expansion and the upstream SOL width) is taken as $w \approx 10$ cm.

Using these measurements and parameters, in the most detached case, the estimated power losses are 100–170 kW, which is significant (8%–13%) compared to an estimated input power (P_{SOL}) of 1.3 MW. This is in reasonable agreement with SOLPS-ITER simulations, which indicate similar power losses from elastic ion/molecule collisions (also shown on figure 15) and which suggest losses of up to 40%–50% of power remaining downstream of ionisation (not shown on plot). The power losses from plasma chemistry (e.g. MAD) are of similar order of magnitude ($\sim 15\% P_{\text{SOL}}$ [8, 16]). Although this power ultimately reaches the vessel walls, it is spread over a much wider area than the target as the neutrals re-associate at the wall. Power losses from plasma-molecular interactions can thus be an important power loss channel in detached conditions.

4.3.2. Momentum losses from elastic plasma-molecule collisions. Volumetric momentum losses play a key role during detachment. Depending on interpretation [8], they are either required for detachment [6], or are essential for maintaining a high upstream pressure (or density) during detachment [7, 51, 52], required for reactor implementations.

Historically, such momentum losses were attributed to a dominance of atomic charge exchange over ionisation, which decays at low temperatures driving momentum losses [6, 7, 44]. However, more recent code investigations [15, 43] argue that the dominant momentum loss is driven by *the same ion-molecule collisions* that result in an increase in rotational temperature and plasma power losses. This is supported by reduced modelling that argues the target temperature is a main driver of the divertor processes, since the molecular density is

increased as target temperature is reduced [53]. These theoretical findings provide a paradigm shift in understanding one of the most fundamental processes during detachment. There is no experimental validation of these processes yet.

However, if *the same* plasma-molecule collisions result in 1) increased gas temperature; 2) plasma power losses (W m^{-3}); and 3) plasma-momentum losses (N m^{-3}), then knowledge about one of these processes could be used to obtain information about the other(s).

To achieve this, we investigate the correlation between plasma power losses *to the molecules* and volumetric plasma momentum losses *to the molecules* from plasma-molecular collisions by summing the accumulated losses cell by cell from a range of SOLPS-ITER simulations.

A strong correlation between both quantities, shown in figure 16, is obtained:

$$\frac{S_{\text{mol}}^{\text{LOS}}}{P_{\text{mol}}^{\text{LOS}}} \approx 0.07 \text{ N/kW}. \quad (11)$$

This implies that the chord-integrated power losses (modelled in section 4.3.1), combined with a ‘calibration’ inferred from the correlation between power and momentum losses in simulations, can be used to infer volumetric momentum losses experimentally, using the equation below. Applying these calibration coefficients, the divertor integrated momentum losses (N) from elastic ion-molecule collisions is estimated and shown in figure 17.

$$S_{\text{mol}} = \frac{S_{\text{mol}}^{\text{LoS}}}{P_{\text{mol}}^{\text{LoS}}} \times 2\pi \int_0^{L_{\text{pol}}} R(s) P_{\text{mol}}^{\text{LoS}}(s) ds. \quad (12)$$

Since the total momentum losses (N) are inferred (also summed for multiple flux tubes), they need to be brought into context by comparing them against the total integrated upstream pressure (N). The upstream profiles of n_e and T_e are integrated areally ($\text{N m}^{-2} \rightarrow N$) to provide this comparison. The pressure upstream is approximated using an exponential profile, whose fall-off-length (λ_p) is related to the heat flux fall-off-length (λ_q) [2, 54]: $\lambda_p \approx \frac{7}{6} \lambda_q$ (see appendix). Integrating this areally, to obtain an integrated pressure leads to:

$$\begin{aligned} p_{\text{int}} &= 2\pi \int_{R_{\text{sep}}}^{\infty} r p(r) dr \\ p(r) &= 2n_e^{\text{sep}} k T_e^{\text{sep}} \exp\left(-\frac{r - R_{\text{sep}}}{\lambda_p}\right) \\ \rightarrow p_{\text{int}} &\approx \frac{14}{3} \pi R_{\text{sep}} k T_e^{\text{sep}} n_e^{\text{sep}} \lambda_q. \end{aligned} \quad (13)$$

λ_q is estimated from MAST scalings [55] and the separatrix density and temperature variation with f_{GW} are obtained from previous analysis in [49]. With $R_{\text{sep}} \approx 1.3$ m in MAST-U, we obtain (figure 17(a) purple line):

$$p_{\text{int}} \approx 12 - 20 \text{ N}. \quad (14)$$

Comparing this areally integrated pressure to the volumetrically integrated momentum losses in each divertor (see

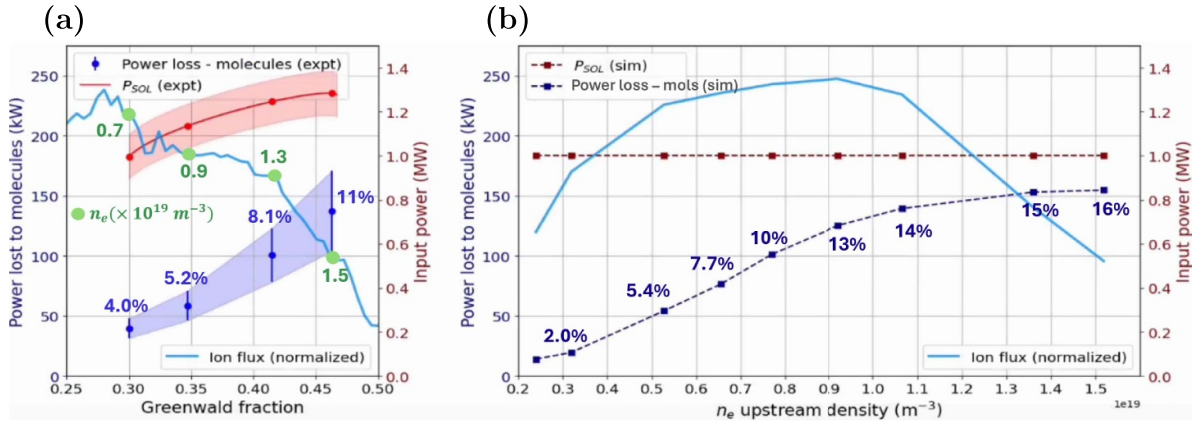


Figure 15. Plot showing the estimated power transferred to the molecules in the experiment (a), and the same value outputted from the simulations (b). The percentages are the corresponding percentages of input power (P_{SOL}) lost in elastic collisions to the molecules. For reference, the blue line shows the normalised target ion flux, and the green circles show the upstream electron density in the experiment.

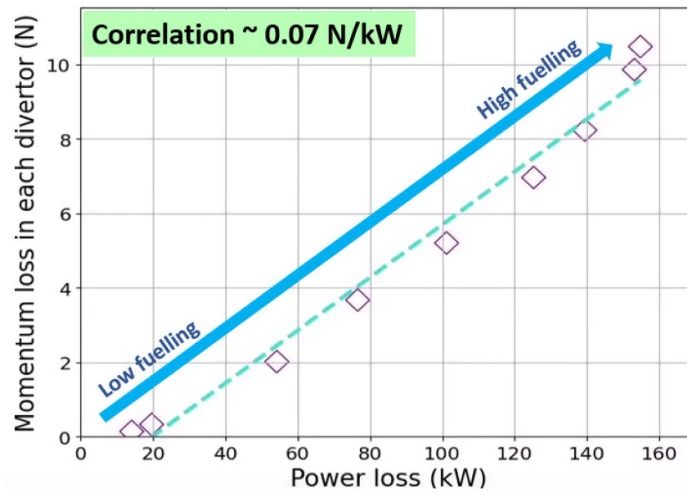


Figure 16. figure indicating the correlation between power and momentum losses to the molecules summed cell-by-cell in SOLPS-ITER simulations for MAST-Upgrade.

figure 17), we see that the majority of the momentum losses (63%) in deeply detached conditions (high fuelling rate) could be explained by elastic ion-molecule collisions. This is consistent with SOLPS-ITER predictions (also shown in figure 17). Interestingly, as also seen in figure 17, SOLPS-ITER predicts that losses due to plasma-atom collisions saturate at relatively low upstream density (before detachment) while plasma-molecule collisions become more and more dominant.

However, it should be noted that this experimental approach is approximate and is a first step. A more complete analysis of the upstream and target pressure—using both upstream and target measurements as well as 2D integrated Data Analysis [56]—is left for future work, such that the inferred volumetric momentum losses can be compared against the total pressure loss obtained.

4.3.3. Limitations of reduced model for power and momentum losses. Although the experimental model provides estimates in quantitative agreement with SOLPS-ITER, there are a number of limitations.

First, the transport time of the molecules or effective transport velocity must be estimated, which cannot be accurately measured. However, it is not expected that this effective transport time changes significantly within the region downstream of the ionisation front and, therefore, it would not impact the trend of the power loss estimates obtained. Secondly, a constant molecular density is assumed in the neutral cloud based on neutral pressure measurements that are significantly away from the divertor plasma, which is not true. The plasma density is also assumed constant whereas, ideally, a measurement is needed. Thirdly, the neutral cloud is approximated as a box downstream the ionisation front. Although the neutral cloud is

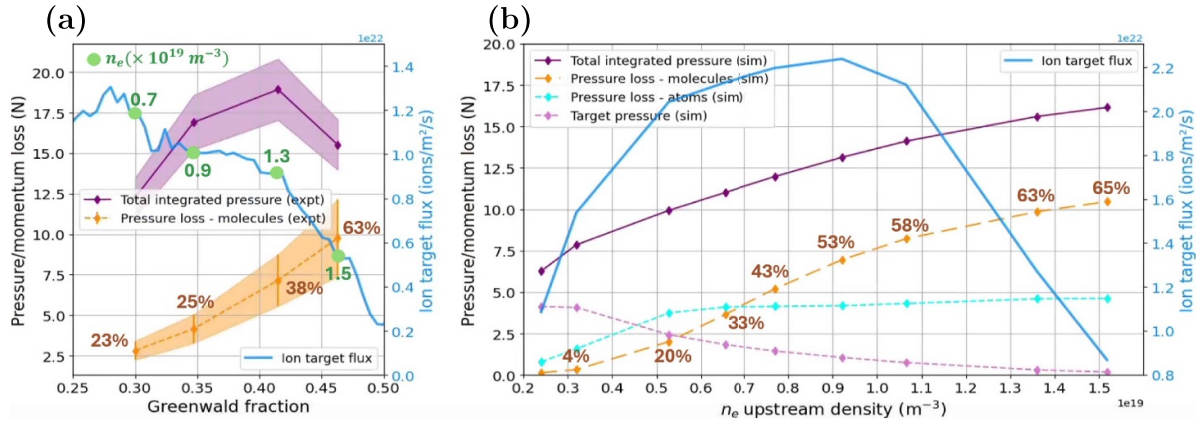


Figure 17. Inferred momentum losses in one divertor (using calibration from SOLP-ITER) compared against integrated pressure at mid-plane SOL for (a) experimental and (b) simulated SXD MAST-U data (including losses from atoms and target pressure). The percentages show the percentage of midplane pressure lost due to elastic collisions with the molecules. The green circles in (a) indicate the upstream electron density.

mostly concentrated downstream of the ionisation front, it also forms around the divertor plasma in these relatively low density/power (and thus large D_2 mean-free-path) plasmas, as can be evidenced from D_2 Fulcher emission occurring throughout the divertor leg, and not just at the target, in attached conditions. The above model may thus underestimate the impact of plasma-molecule collisions in attached conditions and is expected to become more accurate in more strongly detached conditions. Although the neutral buffer description could be made more accurate, this partially defeats the purpose of the reduced model: to provide an intuitive picture of the impact of plasma-molecular interactions, together with quantitative estimates.

An additional further limitation of the volumetric momentum loss estimates is that it relies on a calibration from a set of SOLPS-ITER simulations (with the same power input and geometry) to convert power losses into momentum losses. Further work and model expansion could remove the need for using such a calibration in the future by deriving this relationship between energy and momentum transfer using first principles.

The model would also benefit by being made more predictive. The effect of poloidal flux expansion on power and momentum losses is clearly important, but the current interpretive model does not allow a direct comparison between w and these losses (since there is an interdependency between w and the rotational temperature achieved). The model also currently has no upper bound for the total power or momentum loss.

4.3.4. Implications of power and momentum loss models.

The reduced model used for power and momentum losses has wider implications. In this model, power and momentum losses from plasma-molecule collisions are driven by the ionisation front position, the divertor neutral pressure and

gas temperature. Therefore, the detachment of the ionisation front from the target ($L_{pol} > 0$ m) results in power and momentum losses from plasma-molecule collisions in this model. Since these momentum losses are the dominant volumetric momentum losses, this implies that dominant volumetric momentum losses start to occur when the ionisation front detaches from the target.

In other work, it was argued that the detachment of the ionisation front from the target coincides with the onset of detachment [10, 11] and other work used the ionisation front as a method to control detachment [14]. This model provides a further physics basis for these arguments: real-time control of the ionisation front position, and density of the neutral buffer if possible, is predicted to enable real-time control of the plasma-molecule collisions that drive power and dominant momentum losses.

Recent work shows the *additional volume available* drives the observed differences between longer-legged and shorter-legged divertors [16], consistent with our model. MAST-U experiments indicated similar neutral pressures [57] between the Super-X, Elongated and Conventional divertors. The rotational temperature at *the same poloidal distance to the X-point* is similar between all three geometries. The difference between the three geometries therefore is primarily driven, according to this reduced model, by their difference in $L_{pol} \times R_i$: the longer-legged divertors feature a larger neutral buffer and therefore more plasma-molecular collisions resulting in power losses and volumetric momentum losses. Additionally, in that additional volume available, a colder divertor plasma is present leading to longer molecular lifetimes (i.e. higher rotational temperatures), leading to further enhancements in power and momentum losses.

Assuming that plasma-molecular interactions are the dominant volumetric momentum loss channel, our reduced model can be used to predict differences in the momentum loss between different divertor shapes, which can be compared

against the experimental results shown in [50]. Our model predicts a $\sim 25\%$ reduction of the total momentum loss in the ED compared to the SXD (using $L_{\text{pol}}^{\text{SXD}} = 0.38$ m, $L_{\text{pol}}^{\text{ED}} = 0.26$ m and $R_{\text{f}}^{\text{SXD}} = 1.35$ m, $R_{\text{f}}^{\text{ED}} = 1.15$ m from [57], and accounting for a reduced w by about 30% in the ED). Assuming the volumetric momentum losses in the SXD ($f_{\text{GW}} = 45\%$) are e.g. $\sim 90\%$ (if the effect of atoms is included as suggested by SOLPS-ITER in figure 17), the momentum loss fraction ratio between the SXD and ED $\frac{1-f_{\text{mom,loss}}^{\text{SXD}}}{1-f_{\text{mom,loss}}^{\text{ED}}}$ is expected to be ~ 0.3 , which can be compared with the inferred momentum loss fraction ratios in [50] (0.15 – 0.5). This showcases both the wider implications of the reduced model and provides some confidence in its validity.

4.4. Relevance and implications of this work

Our results indicate that the rotational temperatures in tokamak divertors increase during detached conditions with a subsequent drop at the highest levels of detachment. The transition from attached to detached conditions seems to be the dominant driver of this increase for which we have developed an improved understanding. The rotational temperature is found to be correlated with electron density in many works [20, 21, 24] and our results do not contradict these findings. We find that increasing rotational temperatures during detachment, in a wide range of divertor conditions, can be explained by longer molecular life times, resulting in more plasma-molecule collisions. Such collisions result in significant power and dominant volumetric momentum losses to the plasma.

Power balance is an often researched topic in power exhaust, as more than 90% of P_{SOL} must be dissipated in various reactor concepts [58]. However, power balance studies often indicate that less than 90% of P_{SOL} can be accounted for [59]. Due to the increased area over which the power loading from the neutral atoms to the wall is spread, the plasma power losses from plasma-molecule interactions—which can be tens of percent of P_{SOL} —may not be well diagnosed in such power balance studies. This could explain part of the reason why obtaining power balance is challenging in fusion devices.

Reactors will operate at higher power and density conditions, where mean-free-paths of neutrals are reduced. However, a deeply detached long-legged divertor, with strong neutral baffling, will still have a significant neutral buffer [14, 16]. Whether the importance of plasma-molecular interactions extends to reactor designs is unknown and requires further study. However, given the impact plasma-chemistry can have on reactor-scaled simulations [16], it is likely that elastic plasma-molecule collisions play a key role in reactors with strongly/tightly baffled long-legged divertors. This is because, while power losses resulting from plasma-molecule interaction, although significant, are relatively small compared to pre-detachment losses; and heat deposition from neutrals is unlikely to decrease (and may even increase) as a result of plasma-neutral interaction, we do see in this work that such collisions bring about large volumetric momentum losses. Such momentum losses are critical in detachment to reduce ion target flux and prevent the collapse of upstream density.

This suspicion is consistent with SOLPS-ITER modelling of long-legged, tightly baffled divertors for reactors. Investigating the momentum balance of characteristic STEP simulations [60, 61] suggests that the momentum loss driven by plasma-molecule collisions is either significant or dominant, depending on the level of detachment, consistent with the MAST-U results.

While impurity seeding is key in achieving detachment in reactor designs such as STEP (e.g. $\sim 3\%$ Ar in the SOL) [62], high divertor pressures (e.g. at least $\sim 10 - 15$ Pa) are also required to achieve the required upstream density for detachment without degrading the core. The hydrogenic puffing rate required is expected to far exceed the impurity seeding rate (by a factor > 100 [63]) again indicating the relevance of hydrogenic molecules.

Meanwhile, it is important to note that fuel cycle requirements and detachment control may be impacted by plasma-neutral interactions.

Previous work shows disagreements between the impact of plasma-chemistry in simulations and experiments [8, 11], which are related to errors in the molecular charge exchange rates. The comparisons in this work suggest that there is a discrepancy between the vibrational distribution on which these rates are based, and that measured. This may be due to inaccuracies in the collisional-radiative model used, or the vibrationally resolved setup, requiring further study. However, it is shown that the information that can be obtained on the vibrational distribution using D_2 Fulcher emission is limited. Additional studies are likely required using active laser diagnostic techniques to measure the full vibrational distribution in the electronic ground state are required, which is being developed for linear devices such as Magnum-PSI [25].

Despite these disagreements with modelling, the observations of the impact of elastic plasma-molecule interactions are in agreement with modelling predictions. This provides some evidence that elastic plasma-molecule collisions, and their impact on the divertor plasma, are sufficiently accurately treated in exhaust simulation suites for TCV and MAST-U. However, further verification on such processes is required, particularly in higher power conditions and on metallic devices. Additionally, exhaust modelling suggests that the impact of plasma-molecule interactions during detachment is reduced in impurity seeded conditions [15, 64]—likely as the neutral pressure is reduced—which requires additional study. This information may be used in the future to further corroborate the models and physical picture proposed.

5. Conclusion

Investigating the rotational temperature in a range of different conditions on both TCV and MAST-U indicates, qualitatively, similar behaviour: the rotational temperature rises as the plasma becomes more deeply detached, until the rotational temperature becomes comparable to the plasma temperature. This observation holds true in multiple divertor shapes, external heating levels, baffled and unbaffled conditions, L- and H-mode, H_2 and D_2 , as well as different fuelling locations.

A reduced model is derived to predict the observed increase of the rotational temperature (assuming it is approximately equal to the gas temperature). The gas temperature increases as the lifetime of the molecules is increased in a detached plasma, therefore the plasma undergoes more elastic ion-molecule collisions, resulting in higher gas temperatures. This finding is in agreement with SOLPS-ITER simulations: the molecular gas temperature is driven by ion-molecule collisions and increases during detachment, obtaining quantitatively similar values as the rotational temperatures observed.

Elastic collisions between the plasma and the molecules not only increase the molecular gas temperature, but also have significant impact on the divertor plasma according to SOLPS-ITER simulations. This work confirms the impact of elastic plasma-molecule collisions on the divertor state for the first time experimentally.

Using an approximate interpretive model, the plasma power losses from elastic molecule collisions are estimated using: 1) the rotational temperature (measure of increased collisions with the molecules and energy transfer per molecule); 2) the ionisation front position (size of the neutral buffer during detachment); 3) neutral pressure (estimate of the molecular density). Power losses from plasma-molecule collisions are significant in long-legged divertors, accounting for up to 10%–15% of P_{SOL} in the deepest detached conditions. This provides further evidence of the benefit of long-legged, strongly baffled, divertors that are deeply detached and provides further insights into the significance of non-radiative power losses.

Combining this model with correlations between power and momentum losses obtained from SOLPS-ITER, it is shown that plasma-molecule collisions can result in dominant volumetric momentum losses. These momentum losses are expected to result in a strong target pressure reduction, essential for detachment whilst preventing an upstream pressure collapse.

With these results, this work shows novel insights into the importance of plasma-molecule collisions on detachment, which only become significant if there is a substantial amount of molecules (i.e. substantial neutral pressure) and a substantial spatial extent of the molecular cloud (i.e. detachment front significantly detached from the target). This provides further evidence and understanding of the benefit of long-legged, strongly baffled divertors and supports the limiting of target heat loading via real time ionisation front control.

Acknowledgments

This work has received support from EPSRC Grants EP/W006839/1 and EP/S022430/1. This work has been carried out within the framework of the EUROfusion Consortium, partially funded by the European Union via the Euratom Research and Training Programme (Grant Agreement No. 101052200—EUROfusion). The Swiss contribution to this work has been funded by the Swiss State Secretariat for Education, Research and Innovation (SERI). Views and opinions expressed are however those of the author(s) only and do not necessarily reflect those of the European Union, the European Commission or SERI. Neither the European Union

nor the European Commission nor SERI can be held responsible for them.

Appendix

A.1. Derivation of reduced model for gas temperature increase

We consider the collisions of ions with neutrals. During such a collision, it can be demonstrated that the ion energy loss rate per unit volume is given by:

$$\frac{dE_{\text{loss}}/V}{dt} = 8 \left(\frac{2}{\pi} \right)^{\frac{1}{2}} n_i n_{\text{mol}} \sigma_{\text{rep}} k^{\frac{3}{2}} \frac{\{m_i M (m_i T + M T_i)\}^{\frac{1}{2}}}{(m_i + M)^2} (T_i - T), \quad (15)$$

where m_i , M , T_i , and T are the ion mass, the target particle mass, the ion temperature and the target particle temperature respectively. k is the Boltzmann constant, and σ_{rep} is a representative cross-section for the interaction [35].

Assuming that translational and rotational degrees of freedom are activated in the molecular cloud, then the energy of the molecular cloud per unit volume is given by:

$$E_{\text{cloud}}/V = \frac{5}{2} n_{\text{mol}} T. \quad (16)$$

Noting that the rate of energy gained by the molecular cloud by energy transfer from collisions will be equal to the rate of energy lost by the ions, then, in the case of D^+ ions colliding with D_2 molecules, (or for that matter H^+ ions colliding with H_2 molecules), equation (15) becomes:

$$\frac{d\left(\frac{5}{2} n_{\text{mol}} k T\right)}{dt} = \frac{16}{9\pi^{\frac{1}{2}}} n_i n_{\text{mol}} \sigma_{\text{rep}} k \left[\frac{k(T + 2T_i)}{m_i} \right]^{\frac{1}{2}} (T_i - T). \quad (17)$$

This leads to a collision energy transfer term:

$$\frac{dT}{dt} \approx 0.4 n_i \sigma_{\text{rep}} \left[\frac{k(T + 2T_i)}{m_i} \right]^{\frac{1}{2}} (T_i - T). \quad (18)$$

We now consider loss terms due to destruction and transport.

The rate of energy loss per unit volume due to destruction is given by:

$$\frac{dE_{\text{loss}}/V}{dt} = -\frac{1}{\tau_{\text{dest}}} \frac{5}{2} n_{\text{mol}} k T + \frac{1}{\tau_{\text{dest}}} \frac{5}{2} n_{\text{mol}} k T_{\text{wall}}, \quad (19)$$

where $\frac{1}{\tau_{\text{dest}}}$ is the destruction frequency. The second term replaces the lost molecules at T_{wall} to ensure constant molecular density.

Similarly, the rate of energy loss per unit volume due to transport is given by:

$$\frac{dE_{\text{loss}}/V}{dt} = -\frac{1}{\tau_{\text{transp}}} \frac{5}{2} n_{\text{mol}} k T + \frac{1}{\tau_{\text{transp}}} \frac{5}{2} n_{\text{mol}} k T_{\text{wall}}, \quad (20)$$

where τ_{transp} is the characteristic transit time of molecules in the plasma.

We define an effective loss time τ_{eff} encompassing both loss mechanisms:

$$\frac{1}{\tau_{\text{eff}}} = \frac{1}{\tau_{\text{dest}}} + \frac{1}{\tau_{\text{transp}}}, \quad (21)$$

allowing us to arrive at the following differential equation:

$$\frac{dT}{dt} \approx 0.4 n_i \sigma_{\text{rep}} \left[\frac{k(T + 2T_i)}{m_i} \right]^{\frac{1}{2}} (fT_i - T) - \frac{T}{\tau_{\text{eff}}} + \frac{T_{\text{wall}}}{\tau_{\text{eff}}}, \quad (22)$$

where f is a scalar to account for inefficiency in the energy exchange term—in particular the requirement to maintain a molecular vibrational distribution.

This differential equation forms the basis for our reduced model.

To find a suitable representative cross-section in building our model (in keeping with the derivation of equation (15) from [35]) we consider the energy exchange process at a given plasma temperature. The energy moment associated with the collision operator has the kernel $\sigma v^5 f_{\text{ion}}$, and since $v^5 f_{\text{ion}}$ peaks sharply for a given ion energy, we take the cross-section corresponding to that peak as the representative cross-section. We therefore utilise the cross-section data for ion-molecule collisions from the AMJUEL data files for EIRENE [34] (numerical fit H.1.2.7) rather than the $\langle \sigma v \rangle$ rate coefficient from the same data files (which would be inconsistent with this approach).

A.2. Effective molecular travel speed

The reduced model for the gas temperature increase requires taking into account the transit time of the molecules, $\tau_{\text{transport}}$, which depends on the distance the molecules must travel (e.g. the width of the divertor leg w) as well as the effective speed of the molecules travelling through the divertor leg, v_{eff} .

As the molecules travel through the divertor leg, their kinetic energy increases due to ion-molecule collisions. However, this does not necessarily dictate the effective speed of the molecules transiting through the divertor leg, as their direction is altered upon colliding with ions. As such we assume the kinetics of the molecules are governed by a 1D random walk process and define:

$$v_{\text{eff}} = \frac{w}{\tau_{\text{transport}}}. \quad (23)$$

In this way, we introduce an approximate model to illustrate that the effective speed of the molecule travelling through the divertor is lower than the thermal velocity.

In this random walk, the effective distance travelled is:

$$d_{\text{eff}} = w = \sqrt{N}\lambda, \quad (24)$$

where N is the number of steps taken (number of collisions) and λ is the distance the molecule travels per step. We assume that this distance is equal to the mean-free-path, obtained between two collisions:

$$\lambda = \frac{1}{\sqrt{2}n\sigma}, \quad (25)$$

where n is the relevant particle density and σ is the cross-section.

The actual distance travelled is: $D = N\lambda$ meaning that $D = \sqrt{N}w$.

If $d_{\text{eff}} > \lambda$, it will take:

$$N = \left(\frac{d_{\text{eff}}}{\lambda} \right)^2 = 2w^2 n^2 \sigma^2 \quad (26)$$

steps to travel $d_{\text{eff}} = w$.

The time for one collision depends on the mean-free-path and the *actual* travel speed of a molecule, $\langle v_{\text{th}} \rangle$, which we assume is determined by its kinetic energy:

$$t = \frac{\lambda}{\langle v_{\text{th}} \rangle}, \quad (27)$$

where:

$$\langle v_{\text{th}} \rangle = \frac{1}{\Delta t} \in T_{T_0}^{T_0 + \Delta t} \sqrt{\frac{3k_b T(t)}{m}} dt \approx \sqrt{\frac{3k_b 4T_{\text{final}}}{m_{D_2}}}. \quad (28)$$

We thus arrive at the following useful equations for the total transit time of the molecule:

$$\tau_{\text{transport}} = Nt = \frac{N\lambda}{\langle v_{\text{th}} \rangle} = \frac{\sqrt{2}w^2 n \sigma}{\langle v_{\text{th}} \rangle}, \quad (29)$$

and for the effective speed of the molecules:

$$v_{\text{eff}} = \frac{\langle v_{\text{th}} \rangle}{\sqrt{2}wn\sigma}. \quad (30)$$

It should be noted that this random walk approach is oversimplified (i.e. the path of the molecules is not 1D; if the root-mean-square distance travelled by the molecule exceeds the divertor leg, it is not true that it has transited through the leg). The point, however, is that the effective speed of the molecule travelling through the plasma is lower than the thermal velocity of the molecule due to the various collisions it undergoes with the plasma. The effective speeds and transit times obtained are consistent with other values reported in literature [26].

A.3. Derivation of upstream pressure profile

The upstream pressure profile can be estimated using a characteristic fall-off-width λ_p , based on upstream density and temperature profiles assuming an exponential decay. Furthermore, we assume $n_e = n_i$ and $T_e = T_i$ throughout

$$\begin{aligned} n_e(r) &= n_e^{\text{sep}} \exp\left(-\frac{r - R_{\text{sep}}}{\lambda_n}\right) \\ T_e(r) &= T_e^{\text{sep}} \exp\left(-\frac{r - R_{\text{sep}}}{\lambda_T}\right) \end{aligned} \quad (31)$$

$$\rightarrow p = 2p_e = 2n_e^{\text{sep}} T_e^{\text{sep}} \exp\left(-\frac{r - R_{\text{sep}}}{\lambda_p}\right)$$

$$\frac{1}{\lambda_p} = \frac{1}{\lambda_n} + \frac{1}{\lambda_T}$$

Using the Two Point Model formulation, assuming that 1) all heat transport is driven by conductive transport; 2) no power losses occur upstream; 3) the upstream temperature is much larger than the target temperature ($T_e^{\text{sep}} \gg T_t$), we obtain $T_e^{\text{sep}} \propto q_{\parallel}^{2/7}$. Assuming an exponential decay of both the temperature and heat flux upstream, using their characteristic fall-off-lengths, we obtain $\lambda_T = \frac{7}{2}\lambda_q$ [2, 54].

Further assuming that the target heat flux, density and temperature profile have exactly the same *shape* as the upstream profiles (i.e. $T_t(r) = T_t^{\text{sep}} \exp(-\frac{r-R_{\text{sep}}}{\lambda_T})$, $n_t(r) = n_t^{\text{sep}} \exp(-\frac{r-R_{\text{sep}}}{\lambda_n})$ and $q_{\parallel,t}(r) = q_{\parallel,t}^{\text{sep}} \exp(-\frac{r-R_{\text{sep}}}{\lambda_q})$), the Bohm sheath criterion ($q_{\parallel,t} \propto n_t T_t^{3/2} \propto p_t T_t^{1/2}$) can be used to relate λ_q , λ_p , λ_T . From this, we obtain

$$\frac{1}{\lambda_q} = \frac{1}{\lambda_p} + \frac{1}{2\lambda_T}. \quad (32)$$

Combining this with $\lambda_T = \frac{7}{2}\lambda_q$ results in $\lambda_p = \frac{7}{6}\lambda_q$.

It is important to note that this method is approximate and contains various assumptions that are not valid (heat, pressure and temperature profiles change between upstream and the target, particularly in detached conditions). However, the point of this approach is to obtain rough estimates for the upstream pressure profile using parameters that can be obtained from literature. More quantitative future work, however, should feature a study of the upstream and target pressure profiles to relate the total pressure loss to the inferred volumetric momentum losses obtained from elastic ion-molecule collisions.

ORCID iDs

N. Osborne  0000-0002-3773-6113
 K. Verhaegh  0000-0002-0500-2764
 D. Moulton  0009-0001-8439-9551
 S. Mijin  0000-0002-6114-0256
 H. Reimerdes  0000-0002-9726-1519
 P. Ryan  0000-0002-7133-6156
 N. Lonigro  0000-0001-8581-0384
 R. Osawa  0000-0002-8152-2323
 S. Kobussen  0009-0000-3502-6313
 Y. Damizia  0009-0006-0612-6300
 A. Perek  0000-0002-4117-0298
 C. Theiler  0000-0003-3926-1374
 R. Ducker  0009-0004-3892-9963
 D. Mykytchuk  0009-0004-0398-9712

References

- [1] Verhaegh K. 2018 Spectroscopic investigations of detachment on TCV *Thesis* University of York (available at: <http://etheses.whiterose.ac.uk/22523/>)
- [2] Stangeby P. 2000 The plasma boundary of magnetic fusion devices *The Plasma Boundary of Magnetic Fusion Devices. Series: Series in Plasma Physics* vol 7, ed P. Stangeby (Taylor & Francis)
- [3] Verhaegh K. *et al* 2019 An improved understanding of the roles of atomic processes and power balance in divertor target ion current loss during detachment *Nucl. Fusion* **59** 126038
- [4] Verhaegh K. *et al* 2021 A novel hydrogenic spectroscopic technique for inferring the role of plasma-molecule interaction on power and particle balance during detached conditions *Plasma Phys. Control. Fusion* **63** 035018
- [5] Lipschultz B., Terry J.L., Boswell C., Hubbard A., LaBombard B. and Pappas D.A. 1998 Ultrahigh densities and volume recombination inside the separatrix of the Alcator C-Mod tokamak *Phys. Rev. Lett.* **81** 1007–10
- [6] Stangeby P.C. 2018 Basic physical processes and reduced models for plasma detachment *Plasma Phys. Control. Fusion* **60** 044022
- [7] Krasheninnikov S.I. and Kukushkin A.S. 2017 Physics of ultimate detachment of a tokamak divertor plasma *J. Plasma Phys.* **83** 155830501
- [8] Verhaegh K. *et al* (the TCV Team and the EUROfusion MST1 Team,) 2021 The role of plasma-molecule interactions on power and particle balance during detachment on the TCV tokamak *Nucl. Fusion* **61** 106014
- [9] Verhaegh K. *et al* 2021 A study on the influence of plasma-molecule interactions on particle balance during detachment *Nucl. Mater. Energy* **26** 100922
- [10] Verhaegh K. *et al* (the MAST Upgrade Team) 2023 The role of plasma-atom and molecule interactions on power and particle balance during detachment on the MAST upgrade Super-X divertor *Nucl. Fusion* **63** 126023
- [11] Verhaegh K. *et al* (the MAST Upgrade Team) 2022 Spectroscopic investigations of detachment on the MAST Upgrade Super-X divertor *Nucl. Fusion* **63** 016014
- [12] Wijkamp T. *et al* (the MAST Upgrade Team) 2023 Characterisation of detachment in the MAST-U Super-X divertor using multi-wavelength imaging of 2D atomic and molecular emission processes *Nucl. Fusion* **63** 056003
- [13] Osborne N., Verhaegh K., Bowden M.D., Wijkamp T., Lonigro N., Ryan P., Pawelec E., Lipschultz B., Soukhanovskii V. and van den Biggelaar T. (the MAST-U Team) 2023 Initial Fulcher band observations from high resolution spectroscopy in the MAST-U divertor *Plasma Phys. Control. Fusion* **66** 025008
- [14] Kool B. *et al* (The EUROfusion Tokamak Exploitation Team and the MAST-U Team) 2025 First demonstration of Super-X divertor exhaust control for transient heat load management in compact fusion reactors *Nat. Energy* (<https://doi.org/10.1038/s41560-025-01824-7>)
- [15] Myatra O., Moulton D., Dudson B., Lipschultz B., Newton S., Verhaegh K. and Fil A. 2023 SOLPS-ITER predictive simulations of the impact of ion-molecule elastic collisions on strongly detached MAST-U Super-X divertor conditions *Nucl. Fusion* **63** 076030
- [16] Verhaegh K. *et al* 2024 Investigations of atomic and molecular processes of NBI-heated discharges in the MAST Upgrade Super-X divertor with implications for reactors *Nucl. Fusion* **64** 086050
- [17] Verhaegh K. *et al* (the TCV Team and the EUROfusion MST1 Team) 2023 Investigating the impact of the molecular charge-exchange rate on detached SOLPS-ITER simulations *Nucl. Fusion* **63** 076015
- [18] Chandra R., Holm A. and Groth M. 2023 Impact of vibrationally and electronically excited H₂ on the molecular assisted recombination rate in detached plasma regimes *Nucl. Mater. Energy* **34** 101360
- [19] Holm A., Wunderlich D., Groth M. and Börner P. 2022 Impact of vibrationally resolved H₂ on particle balance in eirene simulations *Contrib. Plasma Phys.* **62** e202100189
- [20] Sergienko G., Arnoux G., Brezinsek S., Clever M., Huber A., Kruezi U., Meigs A.G., Mertens P., Samm U. and Stamp M.

- 2013 Molecular deuterium behaviour in tungsten divertor on JET *J. Nucl. Mater.* **438** S1100–3
- [21] Hollmann E.M., Brezinsek S., Brooks N.H., Groth M., McLean A.G., Pigarov A.Y. and Rudakov D.L. 2006 Spectroscopic measurement of atomic and molecular deuterium fluxes in the DIII-D plasma edge *Plasma Phys. Control. Fusion* **48** 1165
- [22] Fantz U., Reiter D., Heger B. and Coster D. 2001 Hydrogen molecules in the divertor of ASDEX Upgrade *J. Nucl. Mater.* **290** 367–73
- [23] Kubo H., Takenaga H., Sawada K., Nakano T., Kobayashi S., Higashijima S., Asakura N. and Shimizu K. 2005 Spectroscopic study of hydrogen particle behavior in attached and detached divertor plasmas of JT-60U *J. Nucl. Mater.* **337** 161–5
- [24] Fujii K., Oshioka T., Niihama A., Kuzmin A., Shikama T., Kobayashi M. and Hasuo M. 2023 Plasma-parameter dependence of ro-vibrational temperatures for H₂ in LHD divertor *J. Quant. Spectrosc. Radiat. Transfer* **310** 12
- [25] Akkermans G.R.A., Classen I.G.J., Perillo R., van der Meiden H.J., Federici F. and Brezinsek S. 2020 The role of hydrogen molecular effects on detachment in Magnum-PSI *Phys. Plasmas* **27** 102509
- [26] Yoneda N. et al 2023 Spectroscopic measurement of increases in hydrogen molecular rotational temperature with plasma-facing surface temperature and due to collisional-radiative processes in tokamaks *Nucl. Fusion* **63** 9
- [27] Fantz U. and Heger B. 1998 Spectroscopic diagnostics of the vibrational population in the ground state of H₂ and D₂ molecules *Plasma Phys. Control. Fusion* **40** 2023
- [28] Briefi S. and Fantz U. 2020 A revised comprehensive approach for determining the H₂ and D₂ rovibrational population from the Fulcher- α emission in low temperature plasmas *Plasma Sources Sci. Technol.* **29** 12
- [29] Brezinsek S., Mertens P., Pospieszczyk A., Sergienko G. and Greenland P.T. 2002 Molecular and atomic deuterium in the plasma edge of TEXTOR-94 *Contrib. Plasma Phys.* **42** 668–74
- [30] Brezinsek S., Sergienko G., Pospieszczyk A., Mertens P., Samm U. and Greenland P.T. 2005 Characterization of the deuterium recycling flux in front of a graphite surface in the textor tokamak *Plasma Phys. Control. Fusion* **47** 615
- [31] Harrison J. et al 2024 Overview of physics results from MAST upgrade towards core-pedestal-exhaust integration *Nucl. Fusion* **64** 112017
- [32] Duval B. et al 2024 Experimental research on the TCV tokamak *Nucl. Fusion* **64** 112023
- [33] Astashkevich S.A., Käning M., Käning E., Kokina N.V., Lavrov B.P., Ohl A. and Röpcke J. 1996 Radiative characteristics of 3p σ , π ; 3D π^- , δ^- states of H₂ and determination of gas temperature of low pressure hydrogen containing plasmas *J. Quant. Spectrosc. Radiat. Transfer* **56** 725–51
- [34] Reiter D. 2001 The data file AMJUEL: additional atomic and molecular data for EIRENE *Technical Report* (Forschungszentrum Jülich GmbH) (available at: www.eirene.de/html/amjuel.html)
- [35] Cravath A. 1930 The rate at which ions lose energy in elastic collisions *Phys. Rev.* **36**
- [36] Mertens P., Brezinsek S., Greenland P.T., Hey J.D., Pospieszczyk A., Reiter D., Samm U., Schweer B., Sergienko G. and Vietzke E. 2001 Hydrogen release from plasma-facing components into fusion plasmas—recent results from a spectroscopic approach *Plasma Phys. Control. Fusion* **43** A349
- [37] Bryant J. 2025 private communication (University of Liverpool)
- [38] Moulton D., Harrison J., Xiang L., Ryan P., Kirk A., Verhaegh K., Wijkamp T., Federici F., Clark J. and Lipschultz B. 2024 Super-X and conventional divertor configurations in MAST-U ohmic L-mode: a comparison facilitated by interpretative modelling *Nucl. Fusion* **64** 076049
- [39] Wiesen S. et al 2015 The new SOLPS-ITER code package *J. Nucl. Mater.* **463** 480–4
- [40] Ichihara A., Iwamoto O. and Janev R.K. 2000 Cross sections for the reaction $h^+ + h_2(\nu = 0 - 14) \rightarrow h + h_2^+$ at low collision energies *J. Phys. B: At. Mol. Opt. Phys.* **33** 4747–58
- [41] Holm A., Groth M., McLean A., Scotti F., Rognlien T.D., Meyer W.H., Shafer M.W., Wilcox R.S. and Hollmann E.M. 2023 UEDGE-CRUMPET predicted isotopologue effect on atomic and molecular emission in DIII-D high-recycling divertor plasmas *Nucl. Mater. Energy* **34** 3
- [42] Kobussen S. 2023 Collisional radiative modelling with improved cross sections to investigate plasma molecular interactions in divertor plasmas *Internship Report*
- [43] Moulton D., Lipschultz B. and Harrison J. 2017 Detachment onset in MAST-U according to SOLPS-ITER *44th EPS Conf. on Plasma Physics (Conf. Proc.) (Belfast, Northern Ireland)* (available at: <https://info.fusion.ciemat.es/OCS/eps2017pap/pdf/O5.129.pdf>)
- [44] Self S.A. and Ewald H.N. 1966 Static theory of a discharge column at intermediate pressures *Phys. Fluids* **9** 2486–92
- [45] Pitcher C., Goetz J., LaBombard B., Lipschultz B., Weaver J. and Welch B. 1999 The role of friction in SOL pressure balance in Alcator C-Mod *J. Nucl. Mater.* **266** 1009–14
- [46] Henderson S. et al 2024 Validating reduced models for detachment onset and reattachment times on MAST-U *Nucl. Mater. Energy* **41** 101765
- [47] Niemczewski A., Hutchinson I.H., LaBombard B., Lipschultz B. and McCracken G.M. 1997 Neutral particle dynamics in the Alcator C-Mod tokamak *Nucl. Fusion* **37** 151
- [48] Wischmeier M. 2005 Simulating divertor detachment in the TCV and JET tokamaks *PhD Thesis* EPFL (available at: <https://doi.org/10.5075/epfl-thesis-3176>)
- [49] Verhaegh K. et al 2024 Improved divertor performance in strongly baffled, alternative divertors on MAST upgrade (arXiv:2311.08586v2)
- [50] Lonigo N. et al (the WPTE Team and MAST-U Team) 2024 2D electron density profile evolution during detachment in Super-X divertor L-mode discharges on MAST-U accepted (<https://doi.org/10.1088/1741-4326/ae0b90>)
- [51] Kukushkin A. and Pacher H. 2016 The role of “momentum removal” in divertor detachment *Contrib. Plasma Phys.* **56** 711–6
- [52] Pshenov A.A., Kukushkin A.S. and Krasheninnikov S.I. 2017 Energy balance in plasma detachment *Nucl. Mater. Energy* **12** 948–52
- [53] Stangeby P.C. and Chaofeng S. 2017 Strong correlation between D₂ density and electron temperature at the target of divertors found in SOLPS analysis *Nucl. Fusion* **57** 056007
- [54] Faitsch M., Sieglin B., Eich T., Sun H.J. and Herrmann A. 2015 Change of the scrape-off layer power width with the toroidal B-field direction in ASDEX upgrade *Plasma Phys. Control. Fusion* **57** 075005
- [55] Harrison J., Fishpool G. and Kirk A. 2013 L-mode and inter-ELM divertor particle and heat flux width scaling on MAST *J. Nucl. Mater.* **438** S375–8
- [56] Greenhouse D., Bowman C., Lipschultz B., Verhaegh K., Harrison J. and Fil A. 2025 Two-dimensional inference of divertor plasma characteristics: advancements to a multi-instrument bayesian analysis system *Plasma Phys. Control. Fusion* **67** 035006

- [57] Verhaegh K. *et al* 2025 Divertor shaping with neutral baffling as a solution to the tokamak power exhaust challenge *Commun. Phys.* **8** 215
- [58] Zohm H., Militello F., Morgan T.W., Morris W., Reimerdes H. and Siccinio M. 2021 The EU strategy for solving the demo exhaust problem *Fusion Eng. Des.* **166** 112307
- [59] Liu Y.K. *et al* 2020 Power balance investigation in long-pulse high-performance discharges with ITER-like tungsten divertor on east *Nucl. Fusion* **60** 096019
- [60] Osawa R., Moulton D., Newton S., Henderson S., Lipschultz B. and Hudoba A. 2023 SOLPS-ITER analysis of a proposed STEP double null geometry: impact of the degree of disconnection on power-sharing *Nucl. Fusion* **63** 076032
- [61] Hudoba A., Bakes S., Cunningham G., Henderson S., Eriksson F., Marsden S. and Wilson T. 2024 Optimisation of the poloidal field system for advanced divertor configurations in STEP *Nucl. Fusion* **64** 086055
- [62] Henderson S. *et al* 2024 An overview of the STEP divertor design and the simple models driving the plasma exhaust scenario *Nucl. Fusion* **65** 016033
- [63] Osawa R., Newton S., Moulton D., Henderson S., Badicel V. and Hudoba A. 2024 Assessment of the impact of fuelling puff location on divertor impurity compression and enrichment in STEP *Nucl. Fusion* **64** 106007
- [64] Smolders A. *et al* (the TCV Team) 2020 Comparison of high density and nitrogen seeded detachment using SOLPS-ITER simulations of the tokamak α configuration variable *Plasma Phys. Control. Fusion* **62** 125006